

Ubiquitous Molecular Outflows in z□>□4 Massive, Dusty Galaxies. II. Momentum-driven Winds Powered by Star Formation in the Early Universe

Justin S. Spilker 180, Manuel Araven 20, Kedar A. Phadk 20, Matthieu Béthermi 10, Scott C. Chapma 16,7, Chenxing Dong (董辰兴[§]), Anthony H. Gonzale[§], Christopher CHayward[®], Yashar D.Hezaveh¹⁰, Katrina C.Litke¹¹, Matthew A. Malkan¹², Daniel P.Marrone¹⁰, Desika Narayanan^{13,14}, Cassie Reute[®], Joaquin D.Vieira^{3,15,16}, and Axel Weiß¹⁷ Department of AstronomyUniversity of Texas at Austin 2515 SpeedwayStop C1400 Austin, TX 78712, USA; spilkerj@gmail.com ² Núcleo de Astronomía de la Facultad de Ingeniería y Ciendasiversidad Diego Portales V. Ejército Libertador 441 Santiago Chile ³ Department of Astronomy University of Illinois, 1002 West Green Street Urbana, IL 61801, USA Aix Marseille Université, CNRS, CNES, LAM, Marseille, France ⁵ Department of Physics and Astronomyniversity of British Columbia,6225 Agricultural Road/Vancouver,V6T 1Z1, Canada National_Research Councillerzberg Astronomy and Astrophysics071 West Saanich Roat/ictoria, V9E 2E7, Canada Department of Physics and Atmospheric ScienDalhousie UniversityHalifax, Nova Scotia,Canada Department of AstronomyUniversity of Florida,211 Bryant Space Sciences Cent@ainesville,FL 32611,USA Center for Computational Astrophysics latiron Institute, 162 Fifth Avenue, New York, NY 10010, USA Département de Physiquelniversité de MontréalMontreal, Quebec, H3T 1J4, Canada 11 Steward ObservatoryUniversity of Arizona,933 North Cherry AvenueTucson,AZ 85721, USA ¹²Department of Physics and Astronomyniversity of California,Los Angeles,CA 90095-1547,USA ¹³ University of Florida Informatics Institute 132 Newell Drive, CISE Bldg E251, Gainesville, FL 32611, USA ¹⁴ Cosmic Dawn Center (DAWN)DTU-Space,Technical University of DenmarkElektrovej 327,DK-2800 Kgs.Lyngby, Denmark Department of Physics Iniversity of Illinois, 1110 West Green Street Irbana, IL 61801, USA

¹⁶National Center for Supercomputing Application**ts**niversity of Illinois, 1205 West Clark StreetUrbana,IL 61801, USA Max-Planck-Institut für Radioastronomiauf dem Hügel 69,D-53121 Bonn,Germany

Received 2020 August 25; revised 2020 October 22; accepted 2020 October 25; published 2020 December 16

Abstract

Galactic outflows of molecular gas are a common occurrence in galaxies and may represent a mechanism by which galaxies self-regulate theigrowth, redistributing gas thatcould otherwise have formed starsWe previously presented the first urvey of molecular outflows at \(\to > \subseteq 4\) toward a sample of massilvesty galaxies. Here we characterize the physicabroperties of the molecular outflows discovered in our survey. Using low-redshift outflows as a training set, we find agreement at the factor of 2 level between several outflow rate estimates. We find molecular outflow rates of 150-80 $\sqrt[6]{}_{\square}$ yr⁻¹ and infer mass loading factors justelow unity. Among the highredshift sources, the molecular mass loading factor shows no strong correlations with any other measured quantity. The outflow energetics are consistent the expectations for momentum-driven winds with star formation as the driving source, with no need for energy-conserving phases. There is no evidence for active galactic nucleus activity in our sample, and while we cannot rule out deeply buried active galactic nuclei, their presence is not required to explain the outflow energetics in contrast to nearby obscured galaxies with fast utflows. The fraction of the outflowing gas that will escape into the circumgalactic medium (CGM), though highly uncertain, may be as high as 50%. This nevertheless constitutes only a small ction of the total cool CGM mass based on a comparison to z□~□2–3 quasar absorption line studies, but could represent □10% of the CGM metal mass. Our survey offers the first statistical characterization of molecular outflow properties in the very early universe.

Unified Astronomy Thesaurus concepts: High-redshift galaxies (734); Galactic winds (572); Gravitational lensing (670); Galaxy evolution (594)

1. Introduction

Powerful galactic outflows or winds have been widely invoked in the establishmentand regulation of many fundamental observed correlations in galaxie Qutflows driven by supermassive black hole feedback or processes related to star formation (e.g., stellar winds, supernovae; adiation pressure) are thoughtto regulate the growth of both the black hole and the stellar componentof galaxies (e.g., Silk & Rees 1998; Fabian 1999; Gebhardt et al. 2000). Outflows are also invoked (see Somerville & Davé 2015 for a recent review). Recent as an important mechanism regulating the metallicity of galaxies, capable of transporting heavy elements into the circumgalactic medium (CGM)that surrounds galaxies (e.g., Tumlinson et al. 2017). They are also likely necessary to explain the rapid suppression ("quenching") of star formation

in massive galaxies and the resulting global and spatially resolved properties of the stars and gas in quenched galaxies at high redshift (e.g., Tacchella et al. 2015; Barro et al. 2016; Spilker et al. 2018a, 2019; Bezanson et al 2019).

Feedback and outflows are widely viewed as necessary in simulations in order to preventivercooling and consequently overly massive galaxies. Feedback is typically included in ad hoc ways, and prescriptions differ greatly across simulations high-resolution zoom simulations have been able to drive outflows self-consistently (e.g., Muratov et al. 2015; Agertz & Kravtsov 2016), but the galaxy parameter space probed is still limited (usually focusing on Milky Way-like halos). Thus, constraining outflow scaling relations is useful both for testing predictions from high-resolution simulations and for informing sub-grid prescriptions used in large-volume simulations.

¹⁸ NHFP Hubble Fellow.

Outflows appear to be ubiquitous in galaxies, and the winds hereafter GA17). In the distant universe we are unlikely to are known to span many orders of magnitude in temperature and density (e.g., Thompson et al. 2016; Schneider & Robertson 2017), and as such various components of the winds are observable from X-ray to radio wavelengths (e.g., Leroy et al. 2015). The cold molecular component of outflows molecular gas is the raw fuel for future star formation and appears to be the largest component by mass of most outflowsOH doublet has been detected/e presented a first attempt at (see Veilleux et al 2020 for a recent review) The cold gas in outflows is notoriously difficult to reproduce in simulations because the thermal balance of outflowing gas depends on the detailed hydrodynamics and heating/cooling processeson spatial scales much smaller than typically achieved (e.g., Scannapieco 2013; Schneider & Robertson 2017). The molecular outflow properties of large samples of galaxies can thus provide a valuable constraint for cosmological galaxy formation simulations (e.g., Muratov et al. 2015; Davé et al. 2019; Hayward et al2020).

In the first paper in this series (Spilker et al. 2020, hereafter Paper I), we presented the first sample of molecular outflows in assume a flat Lambda cold dark matter cosmology with the z□>□4 universesing Atacama Large Millimeter Array (ALMA) observations of the hydroxyl (OH) 119 μm doublet as an outflow tracer. The sample was selected from the South Polyminosities $L_{\rm IR}$ and $L_{\rm FIR}$ to be integrated over rest-frame Telescope(SPT) sample of gravitationally lensed dusty starforming galaxies (DSFGs), targeting intrinsically luminous galaxies, $\log L_{\rm IR}/L_{\rm II}\sim 12.5$ -13.5. We found unambiguous outflows in 8/11 (~75%) of the sample, approximately tripling the number of known molecular winds at z□>□4. he observationsalso spatially resolved the outflows, and we found evidence for clumpy substructure in the outflows on scales of ~500 pc.

High-redshift DSFGs such as those targeted by our sample, in particular, can offer unique insight into the physics of feedback and its role in galaxy evolution. Their star formation rates (SFRs) and SFR surface densities are unprecedented in the literature (see Rupke et al. 2005), in which a massthe local universe, and approach the theoretical maximum momentum injection rate from stellar feedback beyond which the remaining gas is unbound (e.g., Murray et al. 2005; Thompson et al2005). DSFGs are expected to trace the most massive dark matter halos of their epodiffering insight into galaxy formation in dense environments (e.dMarrone et al. 2018; Miller et al. 2018; Long et al. 2020). They are also one of few viable populations capable of producing massive guiescent galaxies now identified at~ 4, the existence of which implies that the progenitor systems must have experienced powerful and effective feedback in order to suppress star formation (e.g. including the cosmological helium abundance and mu the Straatman et al2014; Toft et al.2014).

Our primary focus in this work is to understand the physical properties of the molecular outflows we have detected at $z\Box$ > responsible for generating the observed absorption profiles. based on the measured OH 119mm profiles. This is made difficult by the fact that the 119mm line opacity is expected to be very high, $t_{OH 119mn}$ 10 (Fischer et al. 2010). In the nearby universe, extensive observations of ultraluminous infrared galaxies (ULIRGs) and obscured QSOs with Herschel/PACS allowed many OH lines to be detected toward in absorption, the inferred energetics obviously depend the same objects, including some transitions with far lower optical depths and excited transitions that can only arise from the warmestand densestegions. With many OH transitions. self-consistent adiative transfer modeling can reproduce all observed line profiles as wells the dustcontinuum emission simultaneously (González-Alfonso 2017;

possesssuch a rich trove of information until the next generation of far-IR space missions become reality. Even with ALMA at the highest redshifts the atmosphereprecludes observations of the full suite of OH diagnosticand the other OH transitions are typically weaker than the 119m groundis of special interest for many reasons, not least of which is thattate lines. It thus behooves us to understand whether and how well outflow properties can be determined if only the 1100 such an analysis in Spilker et al. (2018b, hereafter \$18), which we expand upon here.

Readers interested only in our interpretation of the outflow properties we derive here are welcome to skip to Section 4. which presents ourmain findings and discussion Section 2 gives an overview of our assumed outflow geometry, calculations of outflow properties and the literature reference samples we use as a training set for our own sample galaxies. Section 3 describes the different methods we use to estimate the outflow rates and explores the level of agreement between the methods. We summarize and conclude in Section 5. We $\dot{W}_m = 0.307$ and $H_b \Box = \Box 67 k \bar{m}$ s $^1 \text{Mpc}^{-1}$ (Planck Collaboration et al. 2016), and we take the total infrared and far-infrared 8–1000 and 40–120m, respectively. We assume a conversion between L_{IR} and SFR of SFR = 1.49 ′ 10 $^{10}L_{IR}$, with L_{IR} in L_{\Box} and SFR in M_{\Box} yr⁻¹ (Murphy et al. 2011). Tables of the outflow properties from this workas well as the SPT sample properties from Paper I, are available in electronic form at https://github.com/spt-smg/publicdata.

2. Outflow Assumptions and Literature Reference Sample

2.1. Assumed Outflow Geometry

Where necessarythroughout this work, we assume a conserving outflow with constant outflow rate expands following a density profile $n \mu r^{-2}$. In this geometry, the outflow rate and mass are related through

$$M_{\rm out}^{\rm l} = 4 \rho R_{\rm out}^2 \, m_{\rm H}^{\rm N} \, V_{\rm out} / R_{\rm out}$$
 (1a)

$$M_{\text{out}} = M_{\text{out}}^{\text{TR}} = M_{\text{out}}^{\text{TR}} / V_{\text{out}},$$
 (1b)

with V_{out} the characteristic outflow velocity, R_{out} the outflow inner radius, m = 1.4 the mean mass per hydrogen atom mass of a hydrogen atom hese quantities are fundamentally linked to the column density of gas along the line-of-sight, N we drop the assumption of spherical symmetry, these quantities are also linearly proportional to the covering fraction, the fraction of the full 4π sr covered by wind material as seen from the source. For our sample, in which the outflows are detected strongly on the orientation of the outflow since no absorption can be detected for outflowing material that does not intersect the line of sight to the galaxyRedshifted receding material is also difficult to constrain for our high-redshiftsample. The ALMA bandwidth probes only a limited range of redshifted velocities, and it is possible for the galaxy itself to be optically

thick to emission from the receding material even if the spectral estimation out of an abundance of caution. These sources can at coverage were extended to more redshifted velocities.

As has been discussed extensively in the literature, this assumed geometry leads to more conservative outflow energetics than otherimple geometries (e.g. Veilleux et al. a factor of 3 lower than if the outflow volume is filled with uniform density (which implies a decreasing outflow rate over FWHM□≈□3000 s ¹ PACS instrumentalspectralresolution time for constantflow velocity), and a factor D^r/R_{out} lower than the "local" or "instantaneous" rate if the wind arises from a thin shell of width Δr . We take the characteristic velocity to be V_{84} , the velocity above which 84% of the absorption occurs. This is also fairly conservative: clearly the maximum velocity is not a "characteristic" outflow velocity, but is more robust to uncertainties in the systemic redshift than the median absorption velocity given the deep absorption asystemic velocities present in most of our sources (Paper I). Finally, we width integrated over velocities more blueshifted than take R_{out} to be r_{dust} the effective radius of the dust emission at rest-frame ≈100mm. This radius has been directly measured for the low-redshift literature reference sources by Herschel/ PACS (Lutz et al.2016) and from our lensing reconstructions of the ALMA OH continuum data, and is motivated by our observation that the OH outflow absorption is frequently strongestin equivalent width not in the nuclear regions but toward the outskirts (Paper I).

The momentum and kinetic energy outflow rates are then given by

$$p_{\text{out}} = M_0 V_{\text{t out}}, \quad \text{ff}_{\text{out}} = \frac{1}{2} M_0 V_{\text{t out}}, \quad (2)$$

where the expression for kinetic power assumesnegligible contribution from turbulent (i.e.non-bulk) sources.

Although maps of the molecular outflows at ~500 pc resolution are available for our SPT sample due to their gravitationally lensed nature (Paper), we do not attempt to match, or otherwise accountor, the structures seen in these maps when estimating outflow rates.

2.2. OH Outflow Training Sample

In order to determine whetherand how well the outflow properties for our high-redshift sample can be estimated given the following subsections. For our objects, we provide the sole available OH 119 µm transitions, we compare extensively to low-redshifULIRGs and obscured QSOs with rich OH data and radiative transfer models from Herschel/ PACS. In particular, GA17 self-consistently model 2 nearby IR-luminous galaxies with detections of the OH transitions at 119, 84, 79, and 65 µm, all of which showed either P Cygni profiles or blueshifted line wings in the 119 µm doublet. The 84velocities. Molecular gas masses were estimated from and 65 doublets are highly excited lines with lower levels 120 and 300 K above the ground state that guire an intense and warm IR radiation field to be detected, and the cross-ladder 79 µm doublet has an optical depth ≈40× lower than the 119 µm transition. We supplement this sample with one additional ULIRG with OH radiative transfer modeling (Tombesiet al. 2015; Veilleux et al. 2017), and an additional four sources with outflow rates based on the detection of high-the torus. No source shows evidence of an AGN in the mid-IR velocity CO line wings that were also observed in OH 119 µm. (or in any other data, e.g., Ma et al. 2016), with fractional These four sources have lower typic | and lower outflow rates than the primary OH-based sampleVe considerthese final sources because Lutz et al. (2020) find reasonable agreemenbetween CO-based and OH-based outflow properties, but we exclude them from our later empirical outflow rate presentin our sample or how common they are if so In our

some level be considered akin to a small cross-validation sample, although the dynamic range in outflow properties they span is small.

For all sources, we remeasured various properties of the OH 2020, and references therein). In particular the outflow rates ar \$19 nm spectra in the same way as for our high-redshift sample including the broadening from at these wavelengths. As for our sample, we use the fits to the spectra to measure the velocities above which 50% and 84% of the absorption takes place 1,50 and 1,84, and the "maximum" outflow velocity $V_{\rm max}$ that we take to be the velocity above which 98% of the absorption takes place. We also measure the total equivalent widths of the absorption components as well as the equivalent widths integrated over various blueshifted velocity ranges; for example W_{<-} 200 refers to the equivalent -200 km s ¹. We note that all these quantities are nonparametric and therefore depend little on the exact methods used to fit the PACS spectra.

Outflow Rate Estimates

In this section we detail number of differentmethods we use to estimate the outflow rates forour z□>□4 SPT DSFG sample. For each method presented here, we estimate uncertaintieson the derived outflow rates through a Monte Carlo procedure, repeatedly resampling the measurements within the uncertainties, redoing the fitting analysis, and remeasuring the predicted outflow rates based on the results of each fit. While we provide several empirical fitting formulae that can be used to estimate outflow rates from OH 119 µm data, we caution that the broad applicability of these formulae is questionable. The literature reference sources are not broadly representative of star-forming galaxies (nor is our z > 4sample), consisting solely of IR-luminous galaxies. It is unclear if the conversions we find here can (or should) be extrapolated to less extreme sources.

For each of our methods herewe aim to find correlations between the published outflow rates for our training sample and the measured OH and ancillary galaxy properties, as detailed in observationaldetails and sample properties Paper I, and briefly reprise here. Gravitational lensing magnification factors were measured from lens models of the rest-frame 119 µm dust continuum emission observed by ALMA along with the OH spectroscopy. From simple fits to the OH spectra, we measured basic observed properties such as equivalent widths and CO(2–1) detections of all sources, following Aravena et al. (2016). Total IR luminosities were measured by fitting to the well-sampled far-IR/submillimeterphotometry, which spans rest-frame≈15-600 µm for all sources. We constrain the contribution of active galactic nuclei (AGN) to the total luminosity using rest-frame mid-IR ~15-30 µm photometry from Herschel/PACS sensitive to hotAGN-heated dustnear contributions to the total luminosity $f_{AGN} = 0.1$ –0.45 (1 σ ; mean upper limit $f_{AGN} = 0.25$), depending on the source. It is possible that this method underestimate f_{AGN} for heavily obscured AGN, but we do not know whether such AGN are

Table 1 SPT Sample Outflow Rate and Energetics Estimates

Source	$(M_{\square}^{\text{thin}} \text{ yr}^{-1})$	$M_{\Box}^{\text{thin corr.}}$ out $(M_{\Box} \text{ yr}^{-1})$	M _□ ^{S18} (M _□ yr ⁻¹)	M ^{HC20} out (M _□ yr ⁻¹)	$(M_{\square}^{PLS} \text{ yr}^{-1})$	$(M_{\square}^{\text{joint}} \text{yr}^{-1})$	M _{out} (10 ⁸ M _□)	Pout (10 ³⁵ dyne)	Æ _{out} (10 ⁸ L _□)
SPT0418- 47	>5	100 100	140 ⁺ 190	220 ⁺ 180	170 ⁺⁶⁰	150 ⁺⁸⁰	4.8 4.1	2.2	6.7
SPT0441-46	>6	120 ⁺ 110 60	170 ⁺ 190	270 ⁺ 180	300 ⁺ 170	190 ⁺ 110	8.3 ⁺ 10.3	1.4	2.3
SPT0459-58	>76	740 ⁺ 500 290	430 ⁺ 190	610 240	590 ⁺ 200 150	590 ⁺ 190	12.5 ^{+ 6.3}	20.7	150
SPT0544-40	>48	510 ⁺³⁵⁰	460 ⁺ 230	630 ^{+ 260}	530 ⁺ 160 150	520 ⁺ 160	$6.0^{+3.2}_{-2.0}$	19.4	150
SPT2048-55	>10	180 ⁺ 160	240 ⁺ 180	280 ⁺ 180	240 ⁺ 130	250 ⁺ 60 90	$7.7^{+3.5}_{-3.4}$	3.3	8.9
SPT2132-58	>47	330 ⁺²⁰⁰	340 ⁺ ²⁴⁰ ₂₅₀	570 ⁺³²⁰	660 ⁺ 320	390 ⁺³¹⁰	3.9 4.4	18.4	180
SPT2311-54	>118	720 ⁺ 440 270	510 ⁺²⁰⁰	1290 400	1580 ⁺⁷⁸⁰	790 ⁺ 770	9.3 ⁺ 11.0	44.8	530
SPT2319-55	>33	390 ⁺ 280	280 ⁺ 180	430 210	500 ⁺ 210 150	380 ⁺ 130	$6.4^{+3.1}_{-2.2}$	12.5	86

Note. Outflow rate estimates are described in the text as follows: M_{out}^{hin} , M_{out}^{fhin} Section 3.1, M_{out}^{S18} , M_{out}^{HC20} : Section 3.2, M_{out}^{PLS} : Section 3.3, M_{out}^{joint} : Section 3.4. We use the joint estimates $M_{\text{out}}^{\text{joint}}$ and associated uncertainties through the remainder of the text subsequently dropping the "joint" superscriftor simplicity. We estimate typical uncertainties on and E aut of ~0.4 dex. This table is available in machine-readable format at https://github.com/spt-smg/publicdata.

subsequent analysis, we detail changes to our interpretation that Under the assumption that the absorption is optically thin, would result from a factor of 2 underestimation of AGN (and consequentlecrease in the fraction of L_{IR} arising from star

While our parent sample consists of 11 z > 4 DSFGs, all of which were detected in OH 119 µm absorption, we determined in Paper I that only eight of these show unambiguous evidence where λ and ν are the wavelength and frequency of the for outflows. It is essentially not possible to set upper limits on the outflow properties for the remaining three sourcessince this would require prior knowledge of, for example, the outflow A_{ul} is the Einstein "A" coefficient of the transition, g_u the velocities. Lack of sensitivity is not the issue; all three were detected in OH absorption but ancillary spectralinformation from [C II] or CO data made the OH profiles difficult to interpret conclusively as evidence for outflows. The sources wentegrated optical depth of the absorption profile (e.g., Mangum selected for OH observations are notobviously biased with respect to the full sample of z□>□4 SPT DSFGs in terms of dust mass, or effective dust temperature (Reuter et l. 2020), although they are by no means representative of "typical" galaxies at this epoch.

The outflow ratesmassesand energetics we derive for our high-redshiftsources from allmethods are given in Table 1. These values as well as the SPT DSFG observed properties given in Paper I we use to derive the outflow rates, are available total (H) column density assuming an OH abundance, in machine-readableformat at https://github.com/spt-smg/ publicdata.

3.1. Simple Optically Thin Model

rates for our sources and the literature reference sample assuming the OH 119 nm absorption is optically thin. As the true outflow rate and an opportunity to determine if some overall correction factor to the optically thin outflow rates could allow a more realistic estimate. While for many nearby galaxies other OH transitions with far lower line opacities can be observed (e.g., the 79 nm doublet, or lines of the less abundant 8OH isotopologue), we must instead attempt to find some other quantity that can provide an empirical correction.

the minimum column density of OH molecules, is given by

$$N_{\text{OH}} = \frac{8pQ_{\text{rot}}(T_{\text{ex}})}{I^{3}g_{l}A_{ul}} \frac{\exp(E_{l}/T_{\text{ex}})}{1 - \exp\left(\frac{-h_{n}}{k_{\text{B}}T_{x}}\right)} \grave{O}t(v)dv, \tag{3}$$

transition,h and $k_{\!B}$ are the Planck and Boltzmann constants, degeneracy of the upper energy levelthe lower energy level in temperature units, Q_{rot} the rotational partition function evaluated at excitation temperature T_{ex} and ∂t^{dV} the & Shirley 2015). For the OH 119 nm doublet transitions, $E_1 \square = \square 0 \text{ KA}_{ul} \square = \square 0.138 \text{ s and } g_u \square = \square 6 \text{(Müller et al.)}$ 2001, 2005). Tabulated values of Q_t are available from the NASA JPL spectroscopic database (Pickett al. 1998). We assume an excitation temperatur $\overline{\ell}_{ex} = 100 \text{ K}$ as found in literature OH studies (e.g., GA17); the combination of T_{ex}-dependenterms in Equation (3) varies by about factor of 3 for 50 < $T_{\rm ex}$ < 150. It is then straightforward to calculate $N_{\rm H} = N_{\rm OH}/[{\rm OH/H}]$. We adopt an OH abundance [OH/H] = 2.5 ' 10^{-6} , as commonly assumed in the literature based on OH studies of the Milky Way star-forming region Sgr□B2 (Goicoechea & Cernicharo 2002).

In order to isolate only outflowing material, it is common to We first consider a simple analytic calculation of the outflow integrate the opticablepth over a limited range of velocities. Here we calculate the integrated optical pth over velocities more blueshifted than -200 km s 1, a commonly adopted already discussed, we expect this to be a very bad assumption threshold. Although this is not fast enough to be guaranteed to but this calculation does at least provide a hard lower bound or race only outflowing material, we expect it to largely trace the outflows even in our sample DSFGs that often show broad CO or [CII] emission line profiles (Paper I). Under the assumption of optically thin absorption, the integrated opticadepth over this velocity range is equal to the equivalent width over the same range. In practice, because the outflow rate itself is proportional to $V_{\rm out}$ (Equation (1)), we instead calculate t(v) v dv from our spectral fitting procedure, consequently incorporating the V_{out} term of Equation (1) into the column density calculation directly. This allows us to include a first-order consideration of the shape of the absorption profiles

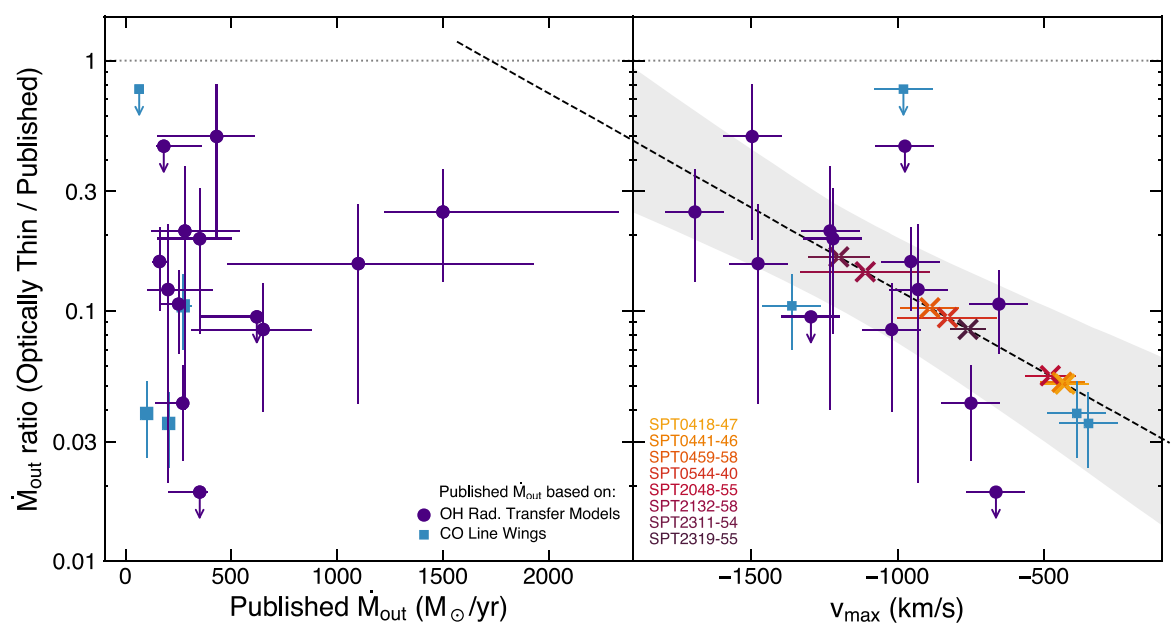


Figure 1. The ratio of optically thin outflow rates to the published values for the literature reference sample (blue symbols) against the published outflow rates (left) and the maximum outflow velocitynax (right). Literature objects with outflow rates derived from multi-transition OH radiative transfer are shown with circles, while those with only CO-based rates are shown as squares. Outflow rates assuming ther mild habs protion is optically thin underestimate the true outflow rates by an amount that is correlated with the outflow velocity. The right panel shows a log-linear fit and 16-84th percentile confidence interval (including an intrinsic scatter of ±0.15 dex) that we use to "correct" the optically thin outflow rates to more realistic estimates using the measured **Alutes tife high-redshift SPT sources (× symbols). The SPT sources in the right panel are placed along the best-fit line according to their measured

in the outflow rate calculation. Finally, because we expect that possible to detect molecular outflow rates of just $\sim 10^{10}$ yr the wind material does not fully cover the source adopt a covering fraction $f_{cov} = 0.3$, the average value determined for the low-redshift reference sample (GA17). We discuss covering alue of the Einstein Afor the ground-state 119 transition, fractions in detail in Paper I, where we estimate covering fractions ranging from a hard lower bound of ~0.1 to upper limits of ~0.7. These covering fractions are also notirectly comparable: GA17 estimate, using their multi-transition OH radiative transfer analysis, while our estimates are based on our as been underestimated. Figure 1 shows. lensing reconstructions with hard lower limits based on spectral There is no obvious trend between the ratio of optically thin analysis. While assuming a different value for f_{cov} would linearly rescale our optically thin outflow rate estimateshis has no impact on our subsequent results, as we explain furtherin different galactic winds. We do, however, identify correlabelow.

We use Equation (1) to calculate the outflow rates for our own and the literature reference samplesFor the reference sample, we use far-IR continuum sizes from PACS 100mm imaging (Lutz et al. 2016), or assume the average size ≈1 kpc we obtain results consistent/ithin the uncertainties from V₈₄ if no data are available. We derive minimum optically thin outflow rates spanning 8–370 M_{\odot} yr⁻¹ for the literature sources and 5–120 M_{\odot} yr⁻¹ for the SPT sample, and correspondingoutflow masses $\log(M_{\rm out}/M_{\odot})$ » 7–8.5. We emphasize thathese values are strong lower limits given the expected high OH line opacities.

Figure 1 (left) shows the ratio of the optically thin outflow rates to the published values from the OH radiative transfer models and CO line wings for the literature sample;upper limits in this plot correspond to those sources that were spatially unresolved by PACS and therefore have upper limits on R_{out}. As expected, the optically thin assumption likely underestimatesthe true outflow rate by a large factor, ≈4–30×□for most source\\$he fact that the outflow rates can be so drastically underestimated is at some level a testament to the sensitivity of OH 119 nm to even minute amounts of

while also removing the need to adopt a characteristic velocity outflowing material: with ALMA at z□>□i♠, principle it is in less than an hour of observing time. This is a consequence of both the relatively high OH abundance and especially the large ~10⁵ times larger than for [OI] 158 nm or ~10⁶ times larger than for low-order CO transitions. The drawback to this sensitivity, of course, is that the line opacities are high and it is not easy to determine by what exact factor the true outflow rate

> to published outflow rate and the published outflow rate itself; evidently the OH 119mm line opacity varies by a large amount tions between this ratio of outflow rate estimates and various measuresof the outflow velocity. Sourceswith the fastest outflows are also the closest to being consistent with optically thin absorption. Figure 1 (right) shows this in term \$ but and V_{50} as well; while V_{max} is somewhatmore difficult to measure (Paper I)t shows the largestlynamic range among the outflow velocity metrics. Such a correlation makes intuitive sense: for a given column density of absorbing gas, if the total gas column extends ovea larger range in velocity, the line opacity per unit velocity interval must necessarily be lower and therefore the line opacity averaged overthe full absorption profile must also be lower. This leads to a less extreme correction factor" needed for sources with very fast outflows.

We fit a simple log-linear function to the data in Figure 1 (right), determining uncertainties on the fit using the same Monte Carlo resampling method we use foall outflow rate techniques. We find a best-fit relation for the outflow rates "corrected" from the optically thin values of

$$\log(M_{\text{out}}^{\text{thin corr.}}/M_{\text{out}}^{\text{thin}}) = m(v_{\text{max}} + 1000) + b, \tag{4}$$

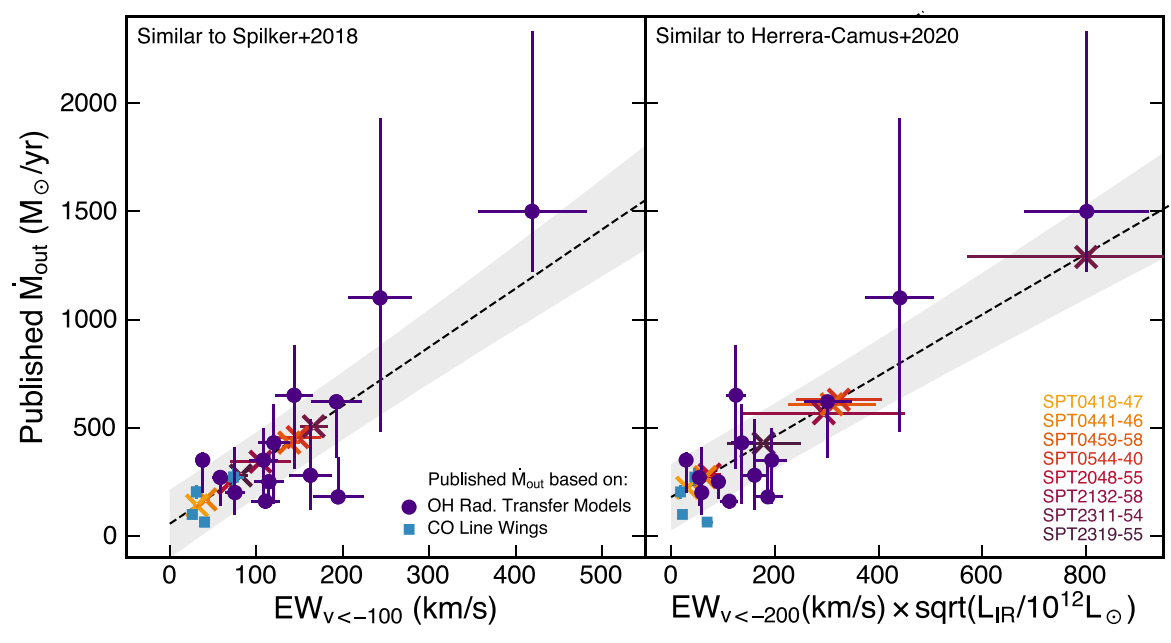


Figure 2. Two simple empirical ways we use to estimate molecular outflow rates, using parameterizations in the style of Spilker et al. (2018b) (left asisuming correlated with the blueshifted equivalent width alone) and Herrera-Camus et al. (2020) (right, assuming an additional dependence interval (including an intrinsic scatter of ±100yr⁻¹; dashed line and gray shaded region). We use these fits and the measured OH 119nm spectral properties to infer outflow rates for the high-redshift SPT sour&essymbols as in Figure 1.

with $m = -6.4^{+1.8}_{-1.7}$ ' 10 4 (km s 1) $^{-1}$ and $b = 0.91^{+0.07}_{-0.06}$, and V_{max} in km s¹. The analysis indicates an intrinsic dispersion of ~0.15 dex around the best-fit relation in addition to the statistical uncertainties/We use this relation and the measured values of V_{max} to estimate the true outflow rates empirically corrected from the optically thin assumption.

We note again that our prior assumption $f_{Qf} = 0.3$ in our calculation of Mout has no impact on our "corrected" outflow between f_{cov} and other galaxy properties in the low-redshift training sample that could influence our outflow rates given the similar to those we used in \$18. differences between the samples (GA17)hile we do find a tentative correlation of cov with L_{IR} (Paper I), we expect those covering fractions to be upperlimits on the true values and stressagain that the methods used between low- and high redshift are not directly comparable Our assume $d_{cov}^f = 0.3$ lies well within the lower and upper limits we expector the true values, so we do not expect this to add substantial additional uncertainty beyond the presentatimates Both the optically thin and the corrected outflow rates are given in Table 1.

3.2. Simple Empirical Estimates

As we expected, the optically thin outflow rates almost certainly severely underestimate the true outflow rateshile we derived a method to correcthese values to more realistic outflow rates, the correction factors remain highly uncertain and in any case the general methodology deserves to be crossscatter beyond the statistical uncertainties; we assume a checked by other methods. We now consider two simple empirical methods to provide alternative estimates of the outflow rates before moving to a more complex empirical method.

In \$18 we made a simple estimate of the true outflow rates using a subsetof the presentliterature reference sources for

which outflows had also been detected in CO emission. In that work we took the OH 119mm equivalent widths for the low-z literature sourcesintegrated overthe velocity ranges where high-velocity wings of CO emission had been detected (GA17), under the philosophy thatoth traced molecular outflows and that the outflows should appear over the same velocity range in both tracersHere we follow a similar vein now including an expanded reference sample stead of individually choosing velocity ranges over which to measure the OH equivalent rates, as a different assumed value propagates directly into b in indths, here we simply fit a linear relationship between the the equation above. There is also no evidence for a correlation published literature M_{out} values and $EW_{\text{c-}100}$ from our remeasured 1119m spectral fits, which gave equivalent widths

> Figure 2 (left) shows the results of this analysis do not force this fit to have a zero intercept. Although this allows the unphysical scenario of positive outflow rates in the absence of any absorption or even negative outflow rates for low equivalentwidths, allowing this freedom in the modelyields a better characterization of the uncertainty at New. We find a best-fit expression for the outflow rate

$$M_{\text{out}}^{\text{518}} = m_{\text{EW}_{\text{<-100}}} + b,$$
 (5)

with $m=2.7^{+0.4}_{-0.5}~M_{\odot}~{\rm yr}^{-1}/({\rm km~s}^{-1})$ and b $\Box=\Box55\Box$ $\pm M_{\odot}^{-1}50$ yr $^{-1}$, the outflow rate in $M_{\odot}~{\rm yr}^{-1}$ and the equivalentwidth in km s⁻¹. We find an intrinsic dispersion of $\pm 150~M_{\odot}~{\rm yr}^{-1}$ around this relation in addition to the statisticaluncertainties that at least applies in the low-W/-- 100, low-Mout regime.At higher Mout there are too few sources to quantify any additional constant $150M_{\odot} \text{ yr}^{-1}$ scatter for all values oEW_{<- 100}.

The OH equivalent width is not expected to be the sole controlling parameterthat predicts outflow rates, of course. Herrera-Camus et al. (2020) (abbreviated HC20) explored an alternative simple parameterization the outflow rates to the product EW_{<- 200} $\sqrt{L_{\text{FIR}}}$. This was motivated by an

expectation that the outflow rate should depend on both the column density of outflowing gas (relatedEM/<- 200) and the size of the source (proportionato $\sqrt{L_{FIR}}$ through a Stefan– Boltzmann type relation)as in Equation (1).

We repeata similar analysis as HC20with a couple small We repeata similar analysis as HC20with a couple small modifications. First, we use $\sqrt{L_{\rm IR}}$ instead of $\sqrt{L_{\rm FIR}}$, which is more readily available for all literature referencesources. Second, we do not fit a line forcing the y-intercept to be zero as done in HC20. Again, this allows us to better understand the uncertainties atow $M_{\rm out}$. Our best-fitrelation for the outflow rate in this way is $M_{\rm out}^{\rm HC20} = m({\rm EW}_{\rm <-200}\sqrt{L_{\rm IR}/10^{12}L_{\rm out}}) + b, \qquad (6)$ again with the outflow rate $M_{\rm out}$ and $M_{$

$$M_{\text{out}}^{\text{HC20}} = m(\text{EW}_{\text{<-200}}\sqrt{L_{\text{IR}}/10^{12}L_{\square}}) + b,$$
 (6)

 $m = 1.40^{+0.21}_{-0.25} M_{\odot} \text{ yr}^{-1} / (\text{ km s}^{-1}) \text{ and} b = 180^{+40}_{-30} M_{\odot} \text{ yr}^{-1}$. We find an essentially identical intrinsic scatter around this relation as before, $\approx 150 M_{\odot} \text{ yr}^{-1}$, where this is assumed to be constant due to the lack of sources with very high outflow rates.

Aside from a more physically justified parameterization, this method also has a slightly higher dynamic range in the abscissa than the \$18-style fit. Between the two methods, we have some preference for the HC20 parameterization. Outflow rates derived from both methods are given in Table 1.

3.3. Multivariate Empirical Estimate

Finally, we consider a more complex empirical model to derive outflow rates. While the analysesin the previous subsection relied on specific linear correlations between observables and published outflow ratesere is no particular reason to choose those specific observables over others apartforest estimators) when some measured observables the from some physical intuition about the likely important parameters. The fact that we find significant additional intrinsic dynamic range of the training sample—that is, when scatter beyond the inferred uncertainties in the previous fits is aextrapolation is required for one or more observables the clue that a more complex modelconnecting the observables and the outflow rates is warrantethdeed, both our reference and high-redshiftsamples have many more known properties than we have yet utilized, both from the OH spectra themselves For our purposes, we use PLS to predict the outflow rates as well as ancillary measurements from otherata. Here we perform one final analysis thatattempts to discern the most predictive relationship between all available measurements and quivalent widths integrated overvarious velocity ranges as the outflow rates, at the expense of linking the resulting relationship to any particular physical meaning.

To explore the complex relationship between outflow rates and all available measurements, we use a "partial least squarewith various numbers and combinations of observables and (PLS) technique (Wold 1966).PLS is both a regression and dimensionality reduction techniquend can be thought f as somewhatof a hybrid between standard multivariate linear regression and principal component analysis (PCA) or singularminimized the mean squared errorin the predicted outflow value decompositionPLS is well-suited to cases such as ours where the number of objects in the reference sample is relatively few but the number of measured quantities for each sample objects large, with many of the measured quantities correlated with each other. In our case, for example, V_{84} and V_{max} encode slightly different information about the shape of the OH absorption profile, they are still strongly correlated: equivalent width were the most predictive of the measured fast outflows are fast regardless of the metric used. While PCAoutflow rates, while $f_{\rm AGN}$ and $r_{\rm dust}$ generally had little techniques are capable of describing the variance in the predictive power, possibly due to the relatively small dynamic observables, not all principal components need be predictive of ange in these quantities in the training and target samples. some other quantity Mout in our case) PLS addresses this by maximizing the covariance between the space of observables published outflow rates for the combination of parameters that and the space of desired predicted quantities. PLS also

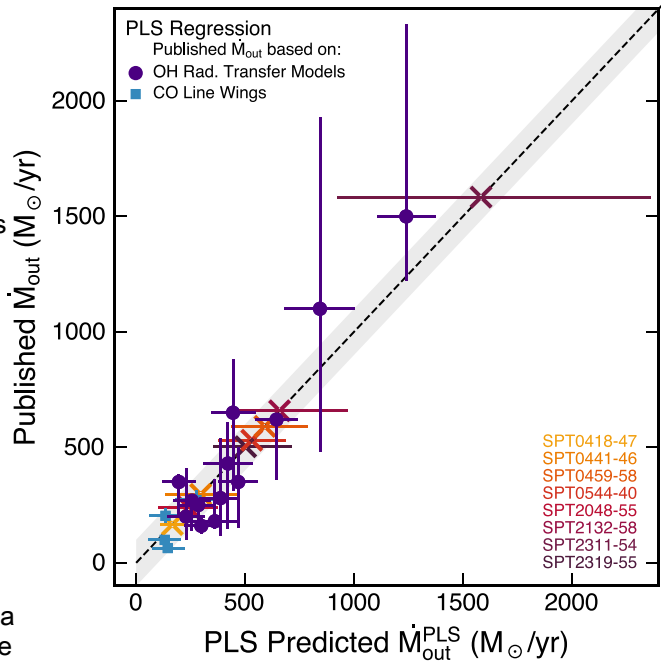


Figure 3. Predicted and measured outflow rates from the empirically based PLS method that does not presuppose any particular functional form between measured properties and the molecular outflow rate. Partial least squares (PLS) is a technique that combines dimensionality reduction with multivariate regression see Section 3.3. The dashed line shows the one-to-one relation while the gray shaded region shows the upper limit to the remaining intrinsic scatter, $\pm 100 \, M_{\odot} \, \mathrm{yr}^{-1}$.

performs better than some other techniques(e.g., random target sample (in this case the SPT objects)lie outside the end this has little influence on our application because the most predictive observable (see below) are well-sampled by the reference objects and extrapolation is not generally required. Mout from a variety of (sometimes strongly correlated) observed properties:several metrics of the OH velocity profiles and well as ancillary galaxy properties such as, roust the AGN contribution to the bolometric luminosity $f_{\rm AGN}$, and the effective dusttemperature we experimented extensively found consistentesults for the predicted outflow rates of the SPT sources in almostall cases. Generally regardless of he observables used, a maximum of four or five PLS components rates of the reference sample (that is, the dimensionality of the problem could be reduced from the number of observables used to four or five, due to covariances between the observables employed).PLS also allows us to understand which observables are most responsible for driving predictions for the outflow rates. Of those we explored the outflow velocity and

Figure 3 shows the comparison between predicted and includes v_{50} , v_{84} , v_{max} , EW, v_{-100} , EW, v_{-200} , EW, v_{total} , v_{IR} , and

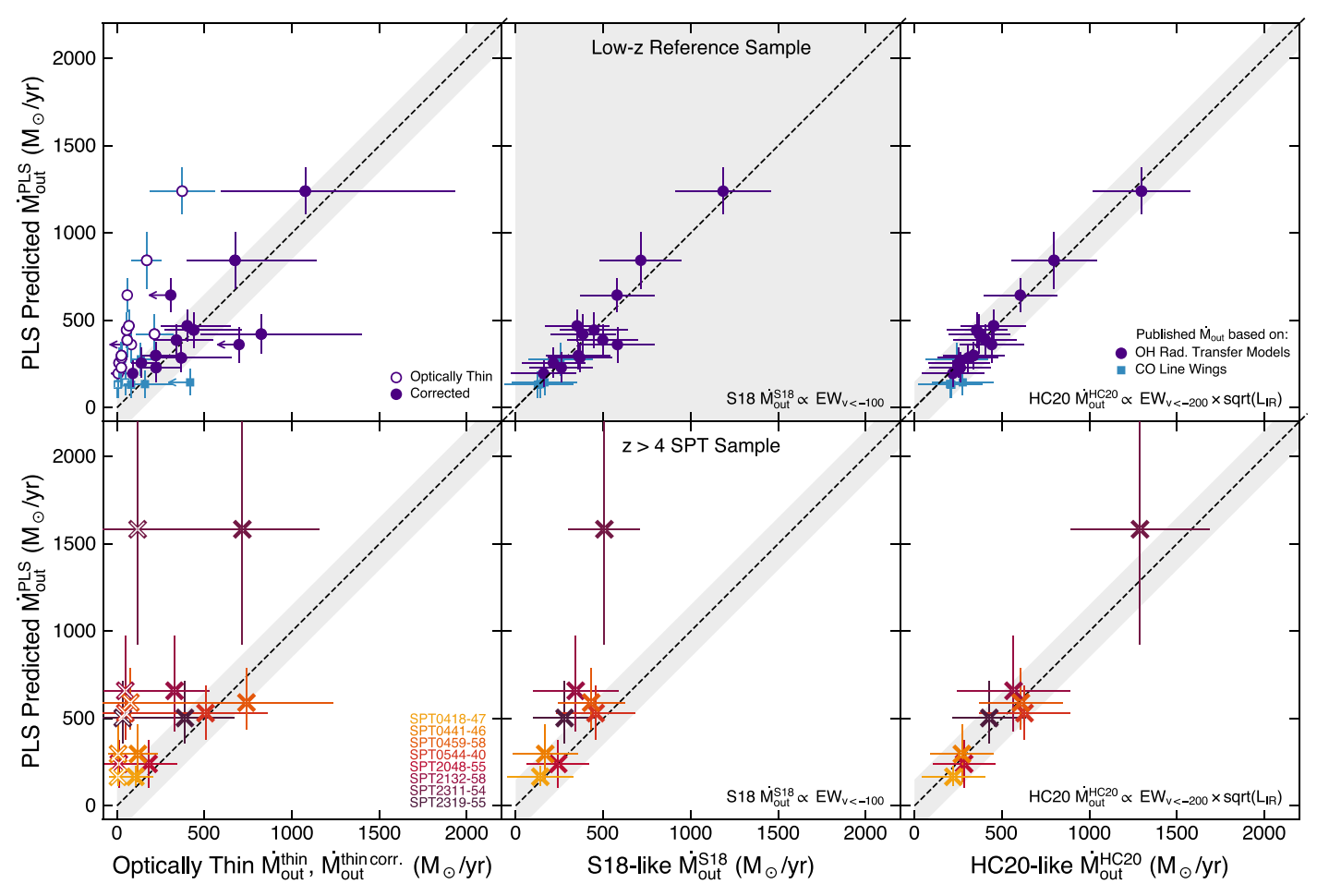


Figure 4. Comparison of all outflow rate estimations we have us Edr easier visualization the literature reference sources are along the top row and the inferred values for the SPT sample on the bottom row. To guide the eye, dashed lines in each panelshow the one-to-one line while the gray shaded region shows ±150 M_{\odot} yr⁻¹ about this relation. The y-axis shows the rates derived from the multivariate empirical PLS technique (Section 3.3), while the columns show the resul from an optically thin estimate (left; Section 3.1) and two simple empirical methods similar to those from S18 (center) and HC20 (right; Section 3.2). In the left-hand column, open symbols are the optically thin outflow rates hile the filled symbols apply the "correction" from Section 3.1.

 f_{AGN} . Interestingly, unlike the previous methods, there is no longer any detectable intrinsic scattebetween the predicted and published outflow rates; the gray shaded region in Figure 3 enerally good agreemeletween the estimators for the SPT rather unsatisfying to necessarily discard allphysical interpretation of the resulting predictions, clearly PLS is capable of spectra and ancillary galaxy properties. translating the complex measurementations into the desired output outflow rates. Predicted outflow rates from this method more detail. This figure shows the outflow rates derived from are provided in Table 1.

3.4. Summary and Method Comparison

We now have four different estimatesfor the molecular outflow rates applied to the high-redshift SPT objects—one corrected from the optically thin assumption, two simple empirical estimators, and one more complex empirical estimate Figure 4 compares these estimates for both the lowredshift reference sample and as applied to our z□>□4 object@greementor disagreementbetween methods and summarizes Note that for the literature sources this figure only compares the constraints we place on the outflow rates. These joint outflow rates predicted from each method to each other; comparisons with the "true" published values can be found in the preceding figures.

Essentially by definition this figure shows good agreement between the various methods for the reference samplince

this sample was used to derive the conversions between observables and outflow rates in the firstlace. We also find illustrates the approximate upper limit on the scatter we can sebbjects, in particular between the multivariate PLS analysis and with the data available, $\approx 100 \, M_{\odot} \, \text{yr}^{-1}$. Although it remains the simpler approach of HC20. Evidently these methods make use of the most alient predictive measurements from the OH

> Figure 5 compares the outflow rates for the SPT sources in each method for each source his figure again demonstrates the generally good agreemebetween methodsalthough the PLS and HC20-like methods tend to yield slightly higher values than the other methods. We also show a joint distribution of the outflow rates created by equally combining the Monte Carlo trials from each method. While this should not be considered a true joint probability distribution of the outflow rates—the methods derive input distributions are hardly independent, for example—it both highlights the level of outflow rates are listed in Table 1, referred to as . We use these joint estimates and associated uncertainties throughout the remainder of the text as our "best" estimates of the outflow rates, subsequently dropping the "joint" superscriptom the notation for simplicity.

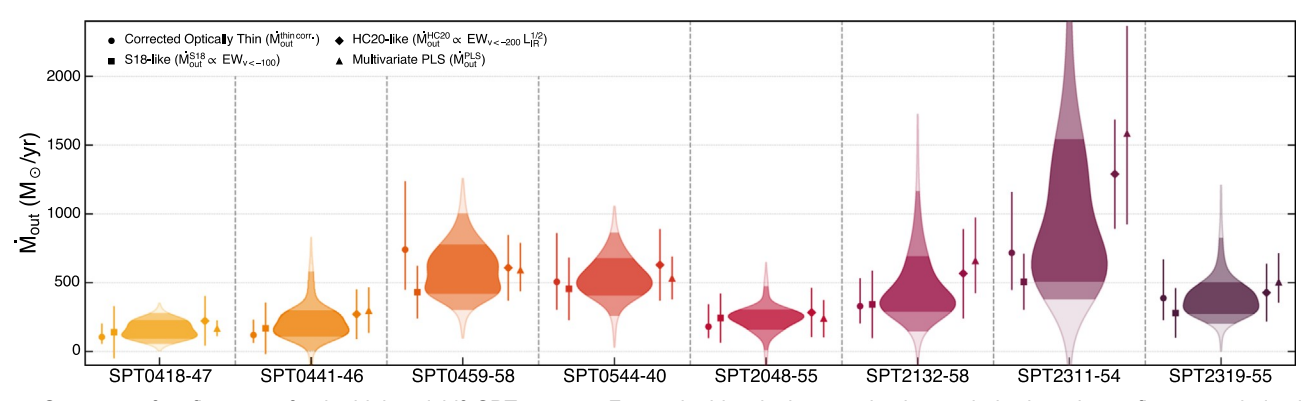


Figure 5. Summary of outflow rates for the high-redshift SPT sources. For each object in the sample, the symbols show the outflow rates derived from each methoindicated, while the violin plot shows the joint distribution from all four methods (weighted equally). Within the violin plots, the darker shaded regions indicate the 68% and 95% confidence intervals.

The joint distributions from each method suggest that we are 2013). While still relatively weak, the strongestcorrelations able to estimate the outflow rates for our sources about the factor of 2 level. The OH-based reference sources have quoted with $L_{
m AGN}$ and $f_{
m AGN}$, suggesting a connection between the uncertainties at the ~50% level; the higher level of uncertainty AGN and wind launching at least in these extreme nearby for our sources reflects the lack of additional OH data for our sample that propagatesinto the scatter seen in the four individual methods and thus into our final joint estimates.

likely underestimated due to systematics in many of the assumptions, from the OH abundance to the assumed geometryearby AGN-dominated systems (described in detail in and outflow history. For our high-redshiftobjects, while our estimates are empirically based, the methods we have described mbols) and those without (empty), as determined by the presume that low-redshift IR-luminous galaxies are sufficiently original authors. We also note that the subsetof low-redshift similar to our targets as to not render these calculations meaninglessWhile the observed characteristics of our sample are contained within the parameter space probed by the reference sample (Figures – 3 and Paper I), it is certainly possible that some other unmeasured quantity has strong influence on the outflow rates that is not accounted for by our methods. Thus, while we propagate the uncertainties on the joint outflow rates in the remainder of the text, it is important to a function of $L_{\rm IR}$. In agreement with Veilleux et al. (2013), we rememberthat these are probably more uncertain by some difficult to quantify amount.

4. Results and Discussion

4.1. Outflow Driving Mechanisms

In low-redshift samples, correlations between outflow velocities and hostgalaxy properties such as SFRs oAGN luminosities have been used to shed light on the physical mechanism(s) responsible for launching the outflows. There are Instead of $L_{\rm IR}$ alone one mightinstead expecthe outflow good theoretical reasons to believe that the energy and momentum imparted to the gas from starformation and/or AGN activity should play a role in driving galactic winds, and should then manifest in the properties of the outflows launched (e.g., Thompson etal. 2015). The second column of Figure 6 Nevertheless, observations of neutral and low-ionizations species show at best weak correlations between outflow velocities and SFR from the local universe to $z \square \sim \square 1$ (e.g., Roberts-Borsani & Saintonge 2019), with any trend mostly due 2016, 2018) for the low-redshift samples and the sizes from Weiner et al. 2009; Rubin et al. 2014; Chisholm et al. 2015; to the weak outflows seen in very low-SFR galaxies (e.g., Heckman & Borthakur 2016).

While this could plausibly be because the neutralutflows are less strongly coupled to the driving source, similarly weak correlations have also been seen for the molecular phase traced w-redshift ULIRGs and QSOs, the strongest correlations with by OH in nearby ULIRGs and QSOs (e.g., Veilleux et al.

between outflow velocities and galaxy properties are found systems.

Figure 6 shows three outflow velocity metric 50, V₈₄, and V_{max} , as a function of I_{IR} , the IR surface densify I_{RR} , I_{AGN} , and We emphasize that for both samples these uncertainties are LAGN, where we now compare our high-redshift objects to the combined sample of low-redshift ULIRGs and QSOs and Paper I). We distinguish between objects with outflows (filled ULIRGs selected for OH radiative transfer modeling by GA17 is skewed toward sources with the fastest outflows, presumably because these were a more viable sample for multi-transition modeling. We return to this point several more times because it propagates into many of the differences we see with the low-z ULIRGs in other outflow properties as well.

> The left column of Figure 6 first shows outflow velocities as see no evidence of a correlation in the expanded sample of nearby galaxiesInterestingly,however,we do see hints of a trend within the $z\Box > \Box 4$ SPT DSFGs when considered alone, with the most luminous sources also driving the fastest outflows. Whether this is a genuine difference between the outflows driven in low- and high-redshift alaxies remains to be seen;a larger sample of high-redshifobjects that spans a wider range in $L_{\rm IR}$ and other properties will be required to understand these tentative differences further.

> velocity to depend more strongly on the IR surface defisity (or similarly the SFR surface density), for example, in cases in shows these quantities for the low- and high-redshift OH molecular outflow samples, where we used far-IR sizes measured from Herschel/PACS imaging (Lutz et al. our lensing reconstructions for the SPT sample (PapelW)e find no convincing evidence of correlation between these quantities even for the SPT sample considered alone.

Of the parameters investigated by Veilleux et (2013) for

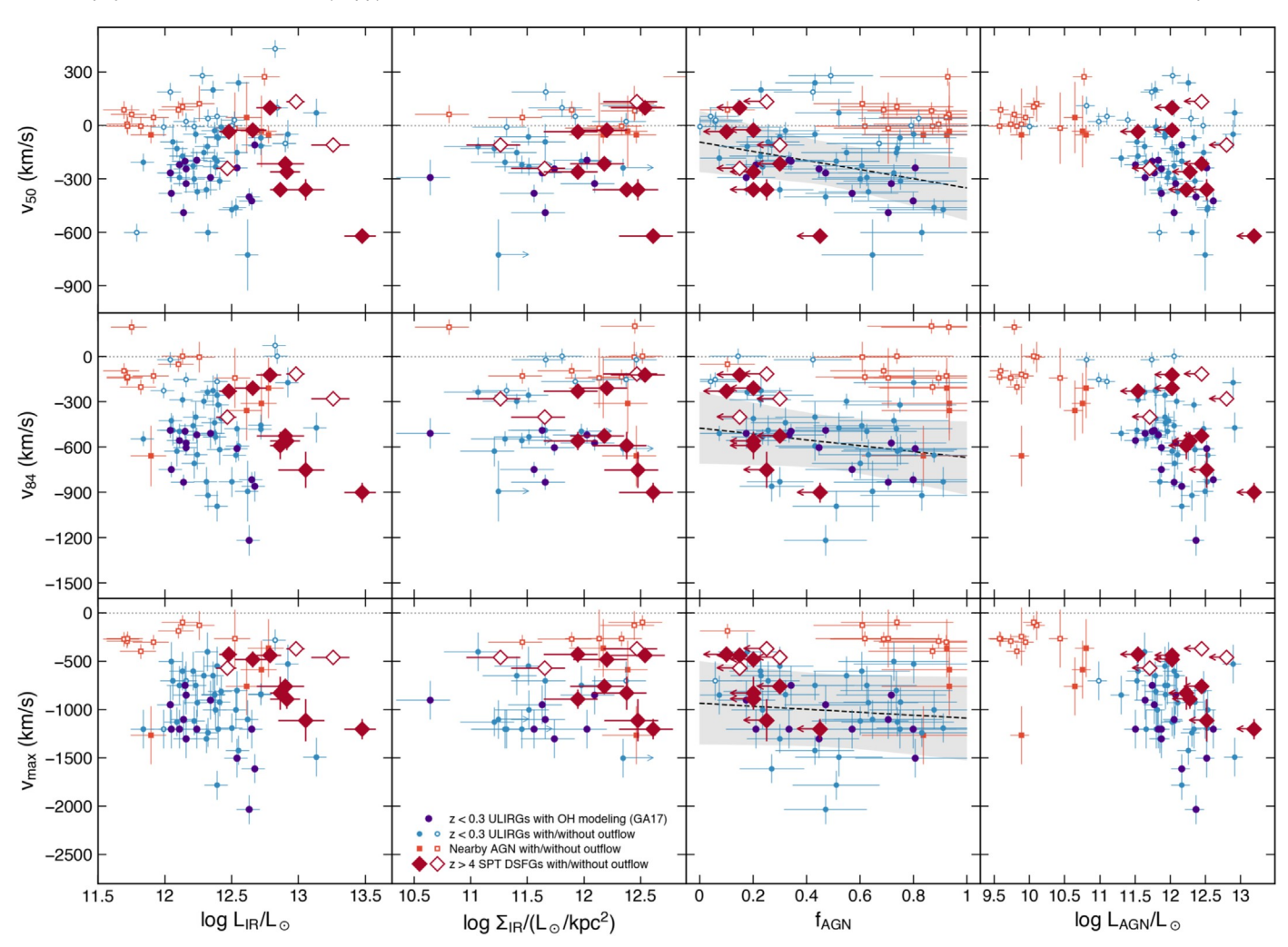


Figure 6. Outflow velocity metrics as a function ϕ_{R} , S_{IR} , f_{AGN} , and L_{AGN} . All velocities are measured from OH 1 ϕ_{R} absorption spectra. Red diamonds show our high-redshift sample, blue circles show the combined sample of nearby ULIRGs and QSOs (Spoon et al. 2013; Veilleux et al. 2013; Calderón et al. 2016; Herre Camus et al. 2020; see Paper I for details), and orange squares nearby AGN-dominated galaxies (Stone et al. 2016). Filled symbols indicate sources with outflows empty those withoutas determined by the original uthors of each study The nearby ULIRGs with OH-based radiative transfer models to measure outflow rates (Section 2.2) are highlighted as larger navy circles. Previous low-redshift work indicated this correlated with the outflow velocities, so in the third column we show simple linear fits with 68% confidence intervals to the low-redshift objects with outflows. While we currently have no evidence of AGN activity in the highredshift SPT sample, our objects are not obvious outliers in these plots, suggesting that we cannot rule out AGN as the driving mechanism of the outflows we have observed.

outflow velocities were found with $f_{\rm AGN}$ and $L_{\rm AGN}$, ¹⁹ which those authors argued could be due to obscuration effects whereby the fastest-moving material was more easily visible infound to be strongly correlated in low-redshift sourcesin the AGN that had already cleared the nuclear regions or were agreementwith Veilleux et al. (2013). We also see some oriented face-on. The subsequent addition of far less luminous relationship between these quantities, namely, sources with low AGN-dominated systems by Stone eal. (2016) agreed with this picture although the number of sources with definite outflows was small. The third column of Figure 6 shows outflow velocities against f_{AGN} . We also fit a simple linear function to the low-redshiftsources with molecular outflows, finding a marginally significant correlation with V_{50} that becomes weaker with f_{84} and f_{max} ; the scatter is clearly large. The limits on f_{AGN} for the SPT sources based on rest-frame mid-IR photometry do not clearly result in these objects being outliers, and they certainly would notbe outliers even if we have underestimate d_{GN} by a substantial amount (Section 3).

Finally, the right column of Figure 6 shows outflow velocities as a function of L_{AGN} , which Stone et al. (2016)

AGN luminosities rarely drive fast outflows. However, we note that while the Stone et al. (2016) sample certainly extends the dynamic range in L_{AGN} probed, this now conflates samples selected in very different ways, with many other possible confounding variables(mass, for example). Regardless, we again find that the limits we can place on L_{AGN} for the SPT sample again do not make them obvious outliers.

In summary, among the SPT DSFGs alone, the total $L_{\rm IR}$ appears to be mosstrongly correlated with outflow velocity, although a largersample size will be required to investigate whether this is genuine. While we recover correlations previously noted in low-redshift work with our larger combined literature sample, the OH outflow velocities appear to be at best with substantialscatter. While we currently have no evidence

¹⁹ These correlations excluded the mosGN-dominated systems where OH was seen purely in emission; none of our sample shows OH in emission either weak indicators of the driving source of molecular outflows, purely or partially.

for AGN activity in the SPT DSFGs and only weak limits on t_{AGN} , our objects are notbound outliers in plots of outflow velocity and AGN properties given the substantial scatter seen among the low-redshiftobjects, and we thus cannotrule out that AGN are responsible for driving the molecular outflows we have observed.

4.2. Molecular Outflow Rate Scaling Relations

A number of recentworks have explored scaling relations between molecular outflow properties and host galaxy properties, compiling samples of now dozens of objects (e.g., Cicone et al. 2014; GA17; Fluetsch et al. 2019; Lutz et al. 2020). While these studies focused exclusively on low-redshift galaxies, we now include our measurementsor the first sample of molecular outflows in the early universe. Our primary comparison samples are the OH-based outflow measurements n nearby ULIRGs from GA17, as before, supplemented with the CO-based sample of Lutz et al. (2020), which extends to lower-luminosity systems. All samples assume the same outflow geometry as discussed in Section 2.1. We note that Lutz et al. (2020) found that OHbased outflow rates tended to be ≈0.5 dex highethan CObased rates in their comparison of galaxies observed in both tracers (while the total outflow masses were very similar) Becausethe CO-based samplespans a different range of parameter space than the other samples, also comments parameter space than the other samples, also comments how our inferences in this section would change if the CO outflow rates were increased by 0.5 dex. We also detail changes to our interpretation that would result from doubling our present upper limits of AGN to try to account for the effects of any heavily obscured AGN that may not be detectable even in the rest-frame mid-IR. It is important to note that none of these samples at any redshift are complete or unbiased; the galaxies typically targeted for molecular outflow observations are highly biased toward luminous star-forming systems and/or quasars.

Figure 7 shows the molecularoutflow rate $M_{\rm out}$ and mass loading factor $h_{\rm out}$ $^{\circ}$ $M_{\rm out}$ / SFR as a function of SFR. We find uniformly sub-unity mass loading factors for the high-redshift DSFGs, although the uncertainties of course remain significant. We would still find loading factors □1 even if we have underestimated oulimits on $f_{\rm AGN}$ by a factor of 2 (which would consequentlylower the SFR). This is a perhaps surprising result—these galaxies are among the most luminou highest-SFR objects known, yet drive relatively weaker outflows than many less luminous nearby galaxies(though again, none of these samplesis complete or unbiased).In particular, despite SFRsa few times higher than the lowredshift OH sample of GA17, the outflow rates we derive do not increase accordingly and the loading factors are consequently lower. At least some of this difference is likely due to the selection for fast outflows in the low-redshift work, but because the outflow rate depends only linearly on the velocity this is insufficient to explain the full difference.

Our sample does appearhowever, to follow the slightly sublinear relationship seen in some low-redshiftudies (e.g., Fluetsch etal. 2019), extended now to an order of magnitude higher SFR and the high-redshift universe. Fitting a power law AGN plays a secondary role in setting the outflow ratence to the combined samples, we find a best-fit relationship $log(M_{out}) = (0.72 \, \mathbb{I} \, 0.05) log(SFR) + (0.5 \, \mathbb{I} \, 0.1)$, with M_{out} and SFR in \dot{M}_{\Box} yr⁻¹ and an additional ntrinsic scatter on the outflow rates of ≈0.25 dex. Thus, we find a transition from $h_{\text{out}} > 1$ to sub-unity values nearan SFR of $\square \sim \square 100$ yr⁻¹.

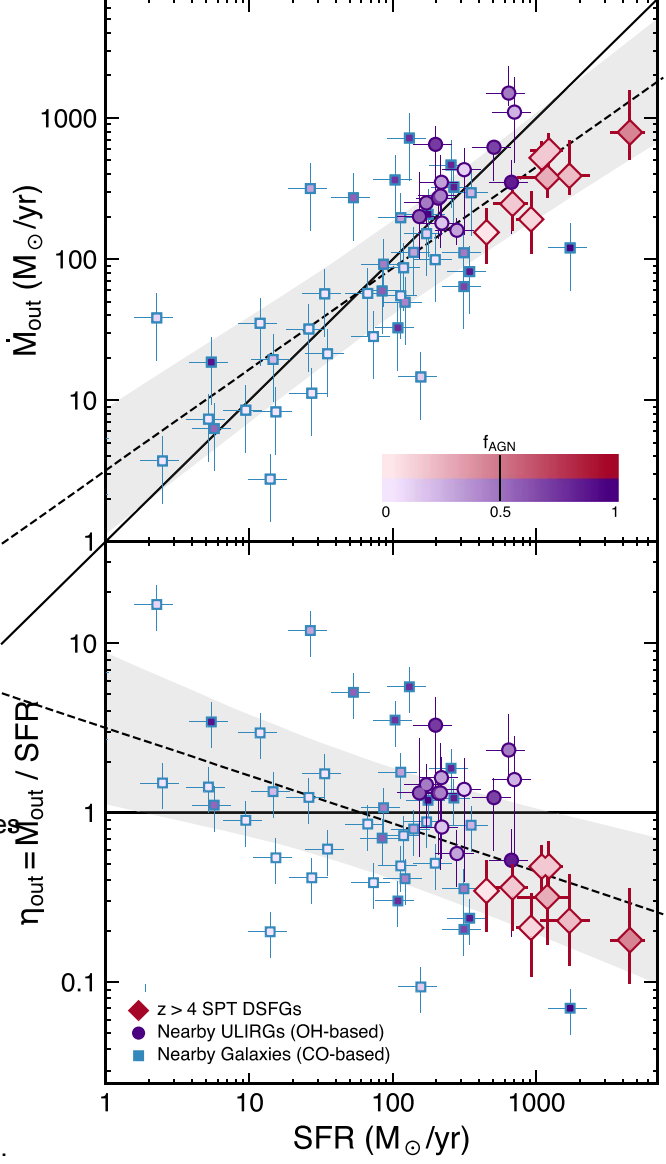


Figure 7. Molecular outflow rates (upper panel) and mass loading factors (bottom) as a function of SFR for the high-redshif PT DSFGs (diamonds), nearby ULIRGs with OH-based outflow rates (circlesand an assortment) spearby galaxies with CO-based outflow rates (squares) into are colored by $f_{\rm AGN}$ (or the limit on $f_{\rm AGN}$, for the SPT sources). Solid lines indicate the one-toone relation in the upper panel $ah_0 d_1 = 1$ in the lower panel. In both, dashed lines and gray shaded regions show the median and 68% confidence interval on power-law fits to the combined samples.

Because of the distribution of the CO-based Lutz et al. (2020) sample in SFR, increasing the CO-based outflow ratesby 0.5 dex would further flatten the power-law slope to ≈0.5 but increase the transition SFR $\Delta t_{tut} = 1$ to $500 M_{\odot} \text{ yr}^{-1}$. On the other hand, if we lowered the SFRs of our sample by doubling f_{AGN} to estimate the effect of a possible highly obscured AGN, the power-law slope would marginally increase to ≈0.8.

Interestingly, we find no evidence that the dominance of an the overall trend with SFR (big) has been accounted for. The points in Figure 7 are color-coded b_{AGN}^{f} , and it is clear that the remaining scatter in the Mout-SFR relationship is uncorrelated with f_{AGN} . This remains a point of some contention in the recentliterature: Cicone et al. (2014) and

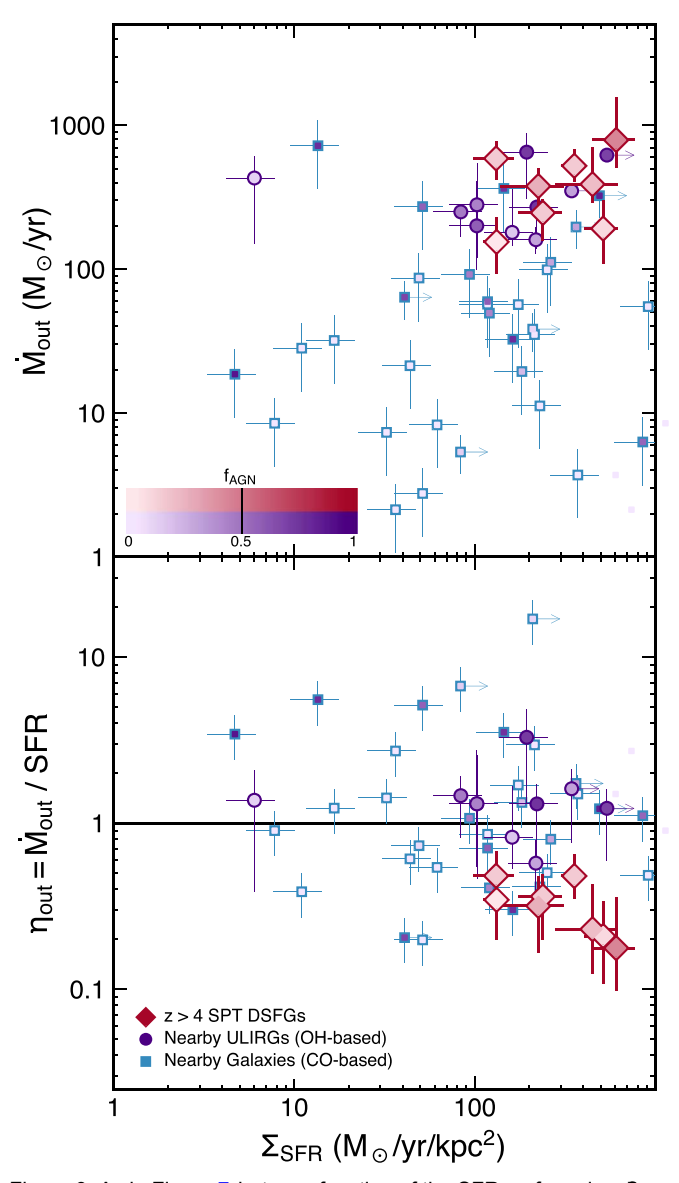


Figure 8. As in Figure 7, but as a function of the SFR surface dens \$\frac{1}{2} \text{SFR}.

Fluetsch et al. (2019) claim a correlation betweenand fagn for $f_{AGN} = 0.7$, while Lutz et al. (2020) found no such correlation, even though both studies use a largely overlapping not complete in S SFR. Severe selection effects stemming set of literature outflow detections (since we use the Lutz et al. from the diverse selection criteria in individual studies 2020 CO-based literature compilation it is no surprise that we comprising the combined literature sample may existincualso find no correlation given the fairly small increasein dynamic range in SFR afforded by our sample). While a thorough analysis ofthis low-redshift discrepancy is beyond the scope of this paper, part of the difference may lie in how the shows a clear relationship between M_{out} and L_{AGN} , with outflow rates were calculated from the CO line wings, as Lutz substantial scatter that increases at legen. The distribution et al. (2020) included only the wings of the broad CO component, while Fluetsch et al. (2019) included the entire broad component (i.e., including emission at systemic

velocities that may not actually be part of the outflow). Figure 8 shows $M_{\rm out}$ and $h_{\rm out}$ as a function of S_{SFR} instead. The SPT sample lies well within the scatter but shows typically not be outliers in the event that our limits on f_{AGN} were lower values of $h_{\rm out}$ at a given S $_{\rm SFR}$ compared to the low-redshift samples. As noted above, this is at least partially explained by the overall sublinear trend between and SFR. Similar to our investigation of outflow velocities with SIR above, we again find no significant correlation between these

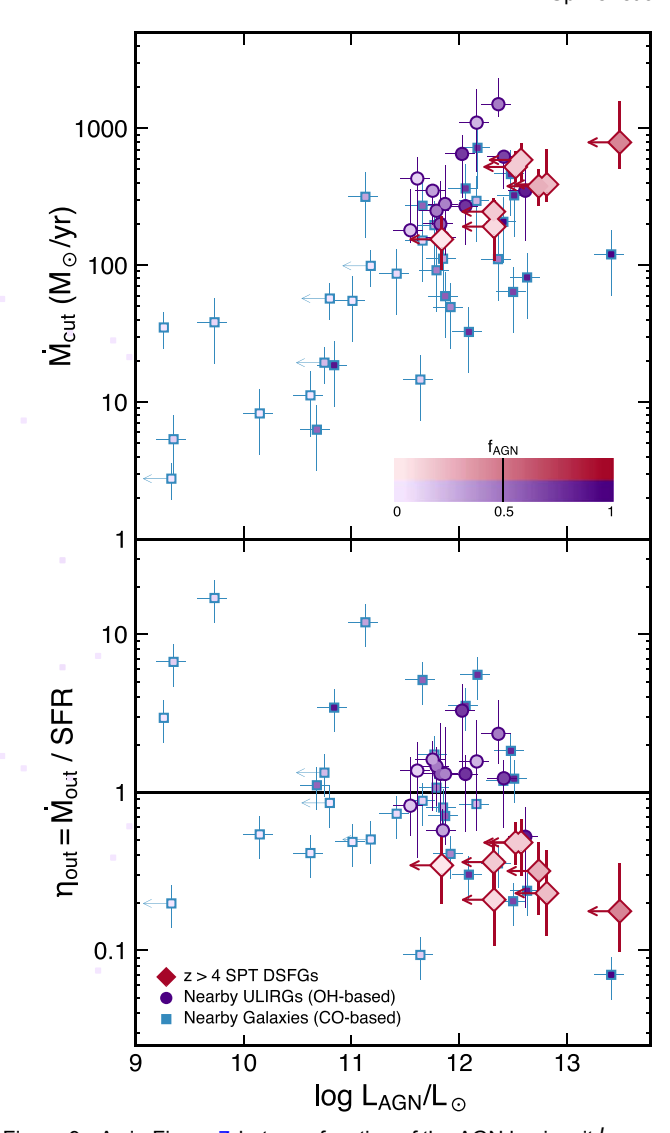


Figure 9. As in Figure 7, but as a function of the AGN luminosity-AGN.

properties, a conclusion that would not change if we increased the CO-based outflow rates by 0.5 dex or adopted 2× higher limits on f_{AGN} for our sample As noted by Lutz et al. (2020), however, the combined literature sample (and our own, clearly)

larly at low S SFR.

Finally, Figure 9 shows f_{out} and f_{out} as a function of f_{AGN} . As seen in previous works the low-redshift combined sample of low-redshift objects in this parameterspace has been discussed extensively in the literature (e.gutz et al. 2020). For our sample, we find that the limits on L_{AGN} from the available rest-frame mid-IR data do not result in the highredshift objects being clear outliers in Figure 9, and they would underestimated by a factor of 2As before in Section 4.1 but from a different perspective, the outflows we have detected do not require an AGN based on mass loading factor scaling relations, but AGN activity also cannot be ruled out in our objects.

4.3. Outflow Masses and Depletion Times

We now turn to estimates of the totalmolecular gas mass contained within the outflows. As described in Section 2.1, we use Equation (1) to calculate the outflow masses for our sample. For the low-redshift samples, we use the original published masses for both the OH-based and CO-based outflows. Recalculating the masses for the low-redshift samples o using our assumed geometry results in <10% differences in the≥ median compared to the published values dditionally, Lutz et al. (2020) found only a 0.06 dex offset and 0.3 dex dispersion between the massefor the low-redshift sources with outflows observed in both OH and COMe make use of the total molecular gas masses forthe low-redshift samples assembled by the original studies, all of which are based on low-J transitions of CO (CO(3-2) or lower). The conversion factor between CO luminosity and It is known to vary based on various galaxy properties (e.g., Bolatto et al. 2013); we accept the values used by the original studies. For the SPT sample, we assume $= 0.8 M_{\odot} (K \text{ km s}^{-1} \text{ pc}^2)^{-1}$, which we have previously found to be appropriate for the IR-luminous galaxies in our sample (e.g., Spilker et al. 2015; Aravena et al. 2016).

Figure 10 shows the molecular outflow masses as a function of $L_{\rm IR}$, as well as the fraction of the total galaxy molecular gas mass contained in the outflows. Not unexpectedly, M_{out} is clearly correlated with IR, as has been previously noted many times in the literature. The z□>□4 SPT DSFG sample has molecular outflow masses in the ratege $M_{\rm out}/M_{\odot}=8.6-9.1$, unsurprisingly on the high end of the local samples. The masses of the two mostntrinsically luminous sources in our sample.SPT2132-58 and SPT2311-54 re perhaps somewhat low in comparison to the extrapolation of the low-redshift samples, but are well within the observed scatter From the lower panel of Figure 10, meanwhile, we find that the molecular outflows in our sample contain 1%–10% of the total moleculargas masses of the galaxies. These values are well within the range typically seen in low-redshift galaxies. Further, we find no discernible trend between M_{out}/M_{H_2} and LIR despite the increase in dynamic range In afforded by our sample.

Figure 11 shows these same quantities as a function of Together, Figures 10 and 11 are effectively the corresponding versions of Figures 7 and 9 M_{sut} instead of M_{out}. As with the outflow rates previously, the current limits Q_{RN} for the SPT DSFGs do not make them obvious outliers in Figure 11. There also shorten the depletion times), gas accretion and/or cooling are no indications from either of these figures that the dominance of the AGN plays any role either in determining M_{out} in general or in defining the scatter M_{out} at a given L_{IR} or LAGN, as evidenced by the lack of secondary trends in these higher or lower depending on the time variability if Lagnary and figures with t_{AGN} .

timescale due to outflows with that due to star formation. Here line, since $M_{\rm H_2}$ is incorporated in both axes. these depletion timescales are defined as the time it would take. For the z \square > \square \$ ample, we find for all sources that for the entire molecular gas reservoir of the galaxies to be removed by outflows or consumed by star formation, assumingunity wind mass loading factors we determine (Section 4.2). the outflow rate or SFR remain constant. That is, $t_{\rm dep,out}$ ° $M_{\rm H_2}/M_{\rm out}$ and $t_{\rm dep,SF}$ ° $M_{\rm H_2}/{\rm SFR}$. These depletion times are only approximate estimates of the important timescales in the evolution of galaxies, given that both outflows and star formation operate simultaneously (which would give shorter depletion times)we ignore molecular gas

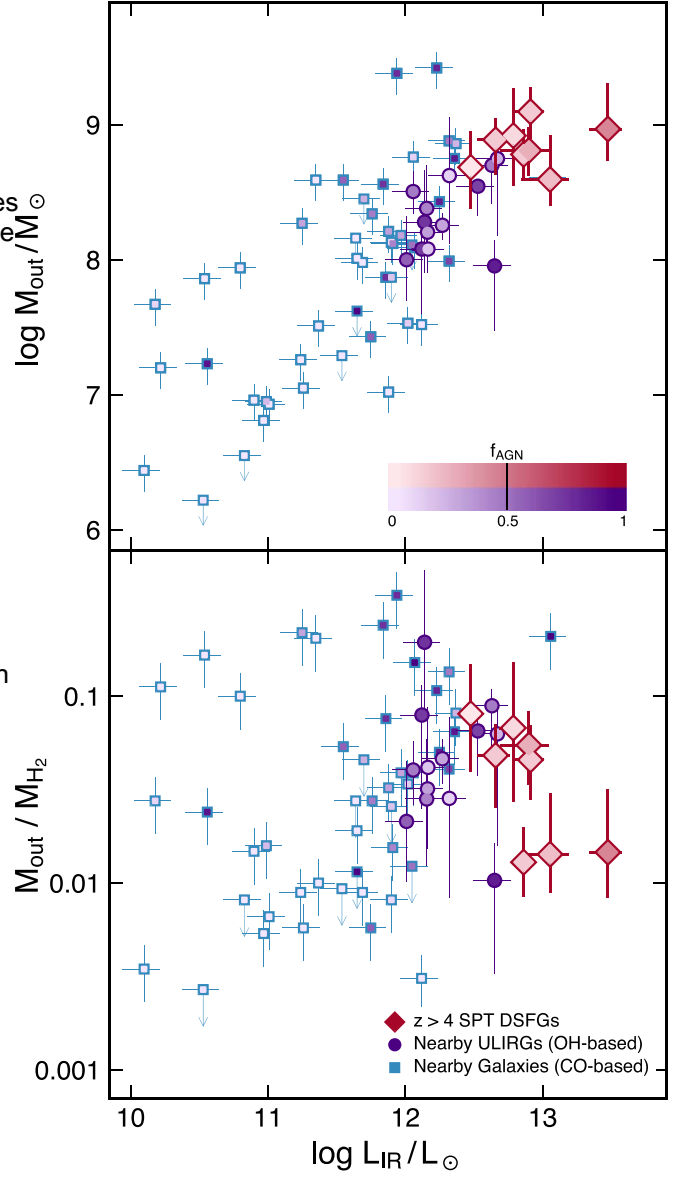


Figure 10. Mass in the molecular phase of outflows (upperpanel) and the fraction of the total galaxy molecular gas mass contained in the outflows (lower panel) as a function of IR. Source symbols and color-coding as in Figure 7.

into the molecular phase are neglected (which would give longer depletion times), and Mout and SFR are not in fact constant over time (which could push the depletion times either SFR). Note that changing estimates oM_{H2} for any object in Meanwhile, Figure 12 compares the molecular gas depletion Figure 12 moves objects diagonally paralled the one-to-one

 $t_{
m dep,out}$ $t_{
m dep,SE}$ a straightforward consequence the sub-This conclusion would also hold if we artificially decrease the SFRs of our sample by doubling as a crude approximation of the effects of a heavily obscured AGN, though the depletion times would be about equal in that case. As before with h_{out} , this places our sample with a distinct minority of the lowredshift samplesWe stress again that all of these samples are destruction due to, e.g., photo-heating or shocks (which would biased toward galaxies and guasarsthat do host powerful

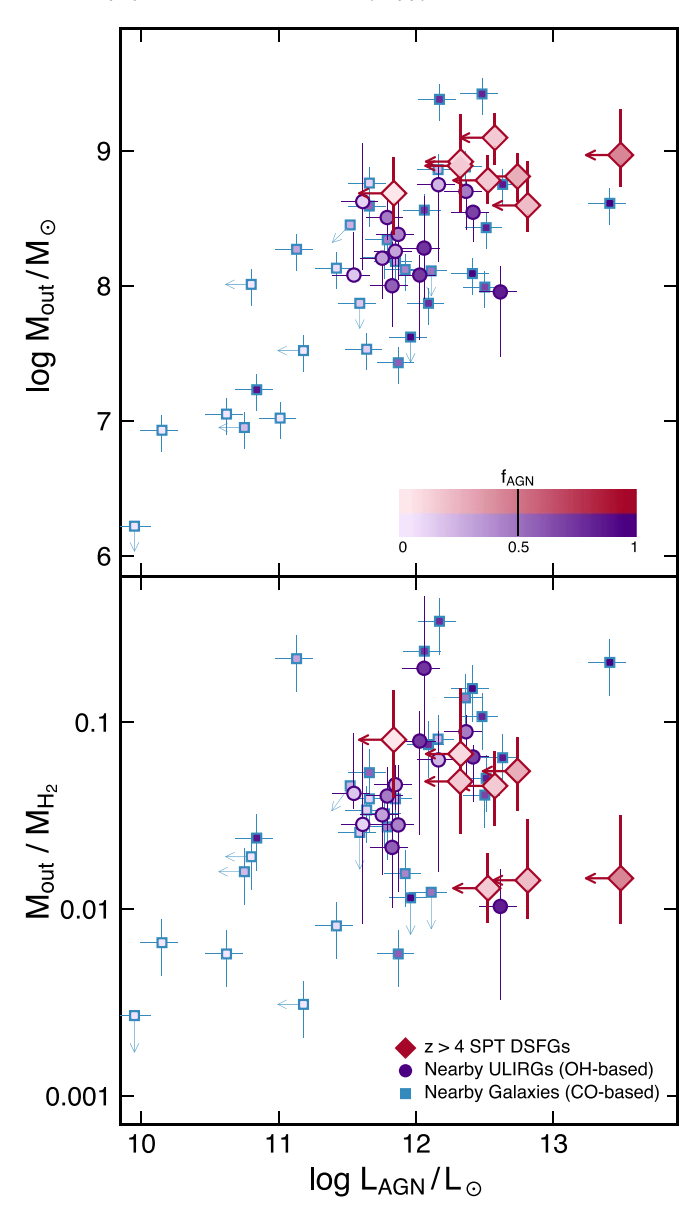


Figure 11. As in Figure 10, but as a function of the AGN luminosity-AGN.

outflows, and these results may notold for objects with less extreme outflows that would be difficult to detect. Unsurprisingly given their very high SFRs and outflow rates, both depletion times are very short, ~10-100 Myr, and the fact that the two timescales are comparable points to the important role that outflows mustplay in regulating starformation in these galaxies.

4.4. Outflow Momentum and Energetics

Galactic winds are often classified as either "energy driven" if radiative losses in the outflowing gas are negligible or "momentum driven" if they are not (regardless of the ultimate source(s) of the energy driving the wind in the former case. the outflow is thought to be launched by the adiabatic expansion of a bubble of hot gas (e.g., Chevalier & Clegg 1985outflow "characteristic" velocity, and some lower velocity Silk & Rees 1998) that either lofts cold gas entrained in the expanding hotwind or (re-)forms cold gas from the swept-up shocked materialat larger radii where the gas can radiatively cool (e.g., Faucher-Giguère & Quataert 2012; Costa et al. 2014and energy were systematically lower.

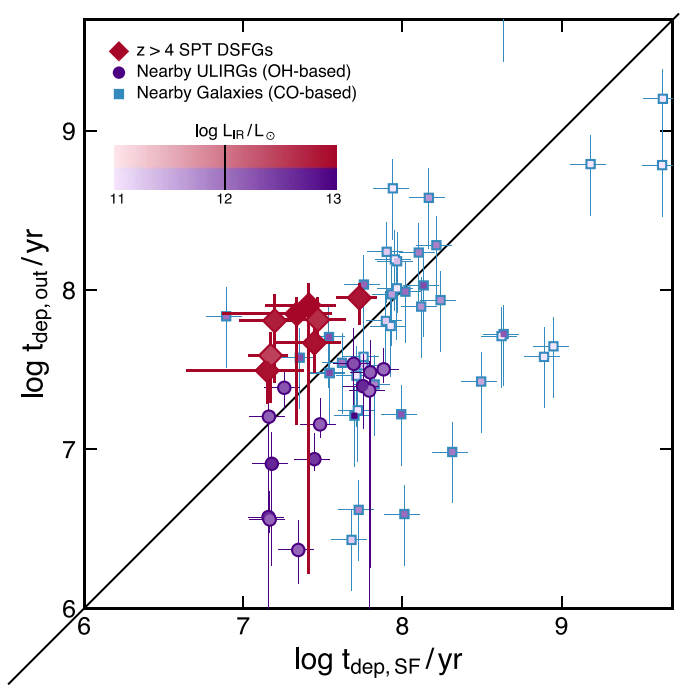


Figure 12. Comparison of the molecular gas depletion timescales due to gas consumption through star formation $h_{\rm H_2}/\rm M_{\rm out}$). Symbols are as in Figure 7 but are now color-coded $h_{\rm H_2}/\rm M_{\rm out}$. The solid line indicates the one-to-one relation. Unlike the majority of low-redshift galaxies, we find shorter timescales for gas consumption by star formation than for removal in molecular outflows (a reflection of the sub-unity mass loading factors we find in our sample; Section 4.2).

Richings & Faucher-Giguère 2018). Similar to the energyconserving Sedov-Taylophase of supernova expansion the resulting momentum in the outflowing gas can be "boosted" well above the radiative momentum flux driving the windh the momentum-driven case in which radiative cooling is significant, momentum transferred to the gas from ram pressure or radiation pressure on dust grains results in gentler acceleration that may allow cold gas to reach large radiand high velocities before it is destroyed (e.g., Murray et al. 2005, 2011; Thompson et al. 2016; Brennan et al. 2018eal winds can of course be intermediate between these cases. both momentum- and energy-driven winds and for winds driven by an AGN or star formation, theoretical models provide estimates of the coupling efficiency between the input momentum and energy and the outflowing gas.

We calculate estimates of the outflow momentum and energy for our SPT sample as described in Section 2 Flor both the low-redshift OH- and CO-based samples we use the original published values of the outflow momentum and energy instead of those derived from our own assumptions in Section 2AI. comparison between the published values and ourstimates indicates thatwe may be overestimating the outflow momentum and energy by ~30% and 70%, respectively, while we find no systematic difference in the mass outflow rateshile still within the substantialuncertainties this probably means that the values of V_{84} we use in Equation (2) are higher than the between V_{50} and V_{84} would provide more accurate outflow energeticsWe continue with our use of V₈₄; our conclusions here would be further strengthened if the outflow momentum

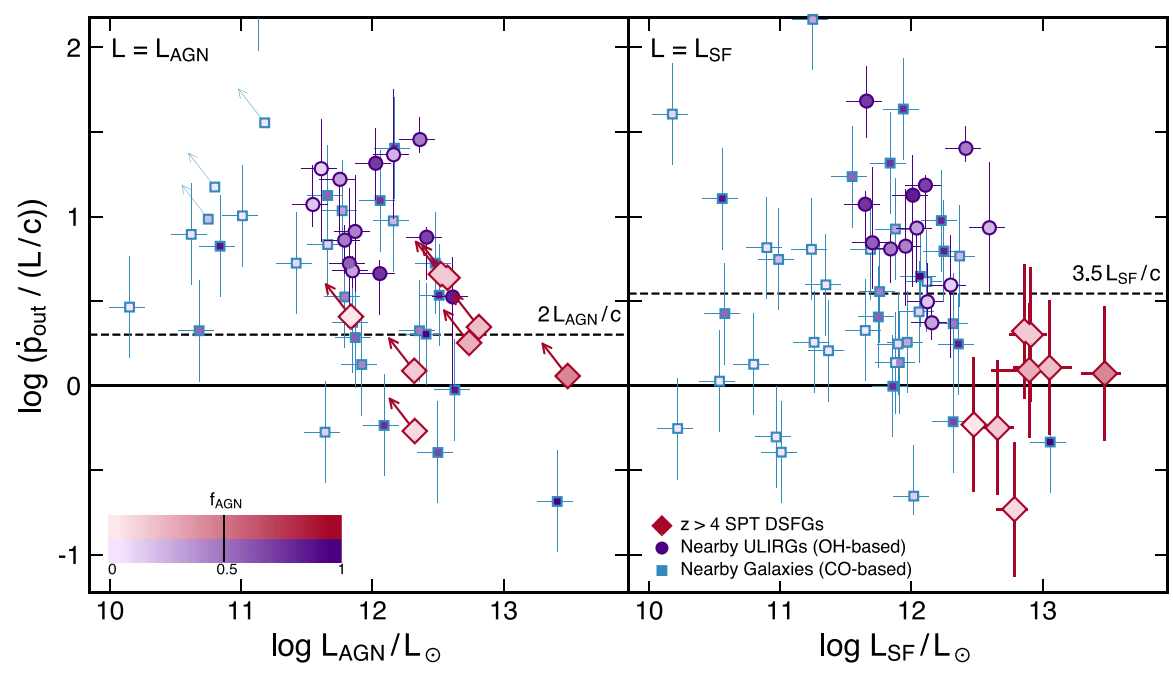


Figure 13. The ratio of the outflow momentum rate to the radiative momentum flux $= L_{F}$ provided by the AGN (left $= L_{AGN}$) or star formation (right; L = L_{SF}) as a function of the AGN and star formation luminosity. Symbols and color-coding as in Figure 7Horizontal dashed lines indicate the approximate maximum momentum attributable to the AGN or star formation in momentum-driven wiffor the high-redshift SPT DSFGsunlike in most local ULIRGs, the radiative momentum flux provided by star formation is fully sufficiently explain the observed outflowsgeither AGN power nor energy-driven wind phases are required.

In Figure 13 we show the fraction of the estimated outflow $(R_{rad} = L \mathcal{F})$ as a function of the estimated luminosities due to AGN and star formation for the sample of molecular outflows assembled from the literature and our high-redshift sample. momentum-driven winds the AGN may provide a momentum rate up to $\sim 2 L_{AGN}/c$, treating both radiation pressure on dust grains and the AGN inner winds as L_{AGN}/c. Meanwhile, a continuous starburstan generate a maximum of ~3.5 SF/c (Veilleux et al. 2005; Heckman et al. 2015) through a molecular outflows in low-redshift galaxies frequently show large momentum boosts ~2–30 above the radiative momentumOH solely in emission in nearby objects (see discussion in provided by the AGN and/or star formation, often taken as evidence that an energy-driven wind phase is required to achieve such large boosts (though see also Thompsonælt 2015, who argue that radiation pressure on dust grains can also Figure 14 shows a similar plot for the outflowing kinetic achieve large momentum boosts in conditions possibly realize power, following our outflow calculations in Section 2.1 Hot in very dusty and gas-rich galaxies).

We find much more modest momentum ratios in our sample of supplying up to about ~5% of the AGN power to the of high-redshiftDSFGs, with maximum momentum boosts of ~2 compared to the luminosity due to star formation and all sources consistent with no momentum boost above the radiative momentum injection at allThis momentum boost is well within the range achievable by radiation pressure on dust in cases where the effective IR optical depth is of order unity (Murray et al. 2005; Thompson et al. 2015). Further, the momentum injection due to star formation alone is fully consistentwith the observed outflow momentum fluxes;no additional radiative momentum from AGN is required. Indeed, it is not clear if the AGN alone could provide sufficient momentum to explain the observed outflows given the current has been taken as evidence that AGN must be primarily limits on L_{AGN}; at least some substantial contribution from star responsible for driving the low-redshift molecular outflows,

formation would be required if AGN are relevant to the outflow momentum rate compared to the total radiative momentum rateenergetics. This result would not change if we redistributed the total luminosity arising from the AGN and star formation by doubling f_{AGN} compared to our current limits, although in that case the momentum flux from the AGN would also be sufficient to drive the outflows we observe. All sources would still show momentum boosts $\Box 3.5 L_{SF}/c$, would still be consistentwith momentum-driving due to star formationand would not show momentum boosts as large as those seen in the local ULIRGs. For our sources to be >1 σ inconsistent with the combination of radiation pressure and the pressure of hot windrough maximum $\sim 3.5 L_{\rm SF}/c$ would require $f_{\rm AGN} > 0.8$ -0.99 material driven by supernova ejecta As seen in Figure 13, depending on the source, far above our current limits from the rest-frame mid-IR. Sources with such high typically show Stone et al. 2016), while none of our sources show OH in emission. This could be taken as evidence that no source in our sample ha $f_{AGN} \square 0.9$.

> energy-driven winds from the AGN are thought to be capable outflows, of which some fraction ~1/2 can plausibly be converted into bulk kinetic energy in the wind (e.g., aucher-Giguère & Quataert 2012; King & Pounds 2015). The mechanical luminosity generated by supernovaeduring a starburst, meanwhile, may reach ~2% of the total starburst luminosity, with perhaps ~1/4 of this luminosity converted into kinetic motion in the interstellar matter (ISM; e.g., Veilleux et al. 2005; Harrison et al. 2014). The outflow energetics in many low-redshiftmolecular winds exceed the expected coupling efficiency to the starburst luminosithile the AGN energetics are in better agreementingure 14). This

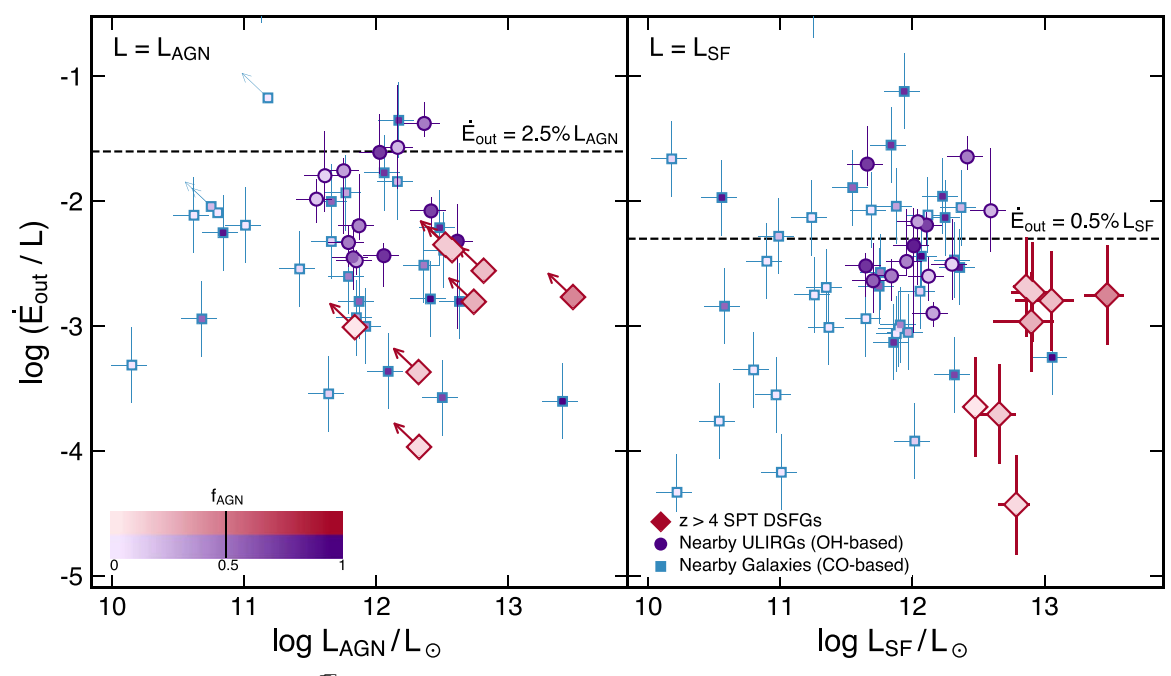


Figure 14. The ratio of the outflow kinetic power to the total luminosity of the AGN (left) or star formation (right) as a function of the AGN and star formation luminosity. Symbols and color-coding as in Figure 7. Horizontal dashed lines indicate the approximate maximum fractions of the AGN or star formation luminosity that can couple to the outflowing gas. For the high-redshift SPT DSFGs, unlike many low-redshift galaxies, the luminosity provided by the AGN is not necessary to explain the outflow energetics; the outflows we have observed are fully consistent with the energy input from star formation alone.

and in combination with the momentum rates in Figure 13, that Both these results are surprising and counter to the these winds must be at least partially energy driven.

In contrast to these low-redshift results, we find that the outflow kinetic energy rates in our z > 4 DSFGs are uniform galaxy growth in massive galaxies, in part due to scaling below the threshold coupling efficiency for supernova-driven winds, and would still be consistent with this coupling efficiency if we adoptlimits on f_{AGN} twice as high (or more) galaxies, we find no need for an AGN in order to explain the as current data indicate. As with the momentum rates, AGN are no lecular outflow energetics we have measured. While our not required in order to explain the observed outflow energetics. Moreover, the AGN in our sample could be an order of magnitude less luminous than the current limits without the outflow kinetic power approaching the theoretical maximum of ~few percent of the AGN luminosity.

the high-redshift molecular outflows we have observed are fully consistent with expectations for momentum-driven winds, with no need for partially or fully energy-conserving phases, and (2) the observed outflow energetics can be fully explained energy rates in our sample. by the momentum and energy provided by star formation alone ULIRGs—both with outflow properties from OH spectroscopy in these galaxies, with no need for additional driving by AGN. We emphasize that we do not conclude that AGN are not responsiblefor driving the observed outflows, merely that AGN are not required to explain the energetics. We note again explain the energetics ofmost of the low-redshift molecular that these conclusions are further strengthened if we adapt somewhatlower characteristic velocity in Equation (2)as it appears may be appropriate by comparison to the OH-based outflow energetics (GA17). Similarly, our conclusions are also not changed in the eventhat our presentlimits on f_{AGN} are underestimated by a factor f 2 (or more) due to AGN so heavily obscured they are not detectable in the mid-IR. In that case eitherthe AGN or star formation could be the ultimate driving source, but the outflow energetics would still not require AGN momentum or energy injection or energyconserving phases.

conclusions typically reached in low-redshift studi@nventional wisdom dictates that AGN are necessary to regulate relations such as that tween black hole mass and galaxy or bulge mass. Yet in our high-redshift rapidly star-forming galaxies, we find no need for an AGN in order to explain the sample objects are more luminous than almastof the lowredshift sources, we have no reason to expect that the outflow energetics should not also increase concomitantly with luminosity. Additionally, the energy-conserving wind mode is generally thought to have the highest coupling efficiency with Taken together, we conclude from Figures 13 and 14 that (1) the ISM, capable of sweeping up a large fraction of the gas in the ISM (e.g., Zubovas & King 2012). Our results,however, show that such high-efficiency energy-driven winds are not necessary to explain the observed outflow momenta and kinetic

> -are particularly striking given their generalsimilarities as highly dust-obscured and IR-luminous galaxiesA17 found that additional energy injection from an AGN is required to outflows in ULIRGs (Figure 14) and that at least partially energy-conserving wind phases are likely necessary to explain the large momentum boosts(Figure 13). Neither of these appears to be true forthe high-redshiftDSFG outflows. We also note that similar conclusion appears to be true for the only other $z\square > \square 4$ object with detected OH absorption, a $z\square = \square 6$. quasar where we expect the total luminosity to be dominated by the AGN (HC20) in contrast to our own sample with only upper limits on L_{AGN} . Although an estimate of the AGN and starburst luminosities separately is not available for this source and the OH detection was low significance, applying the same

outflow property calculations to this source as our sample would also place it in the general vicinity of our sample objects excluding the absorption componentscentered on systemic as long as $t_{AGN} = 0.1$, a condition easily met for luminous quasars.

It is tempting to ascribe at least some of the differences we see compared to the nearby ULIRGs to the overall difference in Arribas et al. (2014). Becausethe detection of absorption luminosities between the low- and high-redshifburces Due to observational limitations the high-redshift objects are typically several times more luminous than the low-redshift ULIRGs. Increasing the luminosity of the ULIRGs would move them down and right in Figures 13 and 14, in the direction that would be required to unify the low- and highredshift objects. However, this would imply that the outflow momentum rates and kinetic powehave essentially reached their maximum in low-redshift ULIRGs and no longer continue to increase in more luminous systems as observed locally (GA17). It is also possible that the physics of outflows is qualitatively different between the low- and high-redshift samples. Multiple simulation efforts have found that star formation-driven outflows become inefficient in massive galaxies at $z \square \square so 1t$ could be that the low-redshift samples are predisposed toward AGN-driven winds by virtue of the fact that they have outflows detected atall (e.g., Muratov et al. 2015; Hayward & Hopkins 2017). It is clear that a larger sample athigh redshift that spans a wider range in parameter the dependencies of outflow energetics on galaxy properties.

play in the low-redshiftsample. As shown in Figure 6, while our sample overlaps with the low-redshiftsamples by most outflow velocities than the low-redshifsample overall, likely because these sources presented a more tractable sample for their modeling. This may weight the low-redshift sample toward AGN-driven (fast) outflows. Additionally, a bias toward fast winds can sharply skew the outflow energetics because the pressure. This would resultin higher outflow escape fractions outflow velocity enters at least linearly in the outflow. outflow velocity enters at least linearly in the outflow momentum rates and at least quadratically in the kinetic power in our sample as a function of the outflow velocity, normalized thus expect that the local ULIRGs with slower outflows would show substantially lower momentum and kinetic energy outflow rates that extend down to the values we find for the SPT sourcesFor the majority of nearby ULIRGs, then, we expect that the outflow energetics would also be consistent with our sample, and SPT2319-55 which has an atypically low momentum-driven winds that do not require additional energy injection from the AGN.

4.5. Fate of the Outflowing Gas

The molecular outflows we have observed could plausibly affect the host galaxies overcosmologicaltimescales, especially if large fractions of the cold gas in the outflows travel at matter halo virial radius. In the latter case, now unbound, the gas may neveragain be available for star formation. In the former, the gas becomes part the CGM and could recycle back into the galaxy unless continued energy injection or shockery wide range in estimated galaxy escape fractionsfrom heating prevents the gas from cooling and condensing (see Tumlinson et al.2017, for a recent review).

We make a simple estimate of the fraction of the outflowing. The escape fraction shows no obvious correlation 始悔 or molecular gas that will escape the host alaxies by assuming the outflowing mass as a function of velocity is directly

proportional to the equivalent vidth as a function of velocity. velocities (Paper I). To estimate the galaxy escape velocity for each sourcewe assume a sphericasothermalmass distribution truncated at a maximum radius $r_{\text{max}}/r = 10$, following requires the presence of continuum emissione take r to be the circularized effective size ofthe dust emission from our lensing reconstruction & We estimate galaxy masses from total molecular gas masses based on CO(2-1) bservations, assuming a typicalgas fraction for DSFGs atthese redshifts (Aravena et al. 2016). These masses are in reasonable agreement with simple dynamical mass estimates using the available [QI] or CO line widths and the lens model sizes (e.g., Spilker et al.2015). We find escape velocities for our sources ranging from $\sim 400-1000$ km s⁻¹ (median ~ 700 km s⁻¹), which agree reasonably well with other simple estimates scaling from the CO or [C] line widths or assuming pointlike mass distributions withir Gust. Given the uncertainties in mass and shape of the gravitational potential, we estimate typical uncertainties on the galaxy escape velocities of ≈40%.

In this calculation, we ignore any additional deceleration of the outflow caused by sweeping up additionalmaterial. We have also implicitly assumed thatthe outflowing material is located at a typical distance from the galaxy center equal to the space than current observations will be required to understand dust continuum emitting size, which seems reasonable based on our lensing reconstructions of the outflow materiaPaper I), There is also a probable selection effect that appears to be a but we cannot rule out that much of this material is located deeper within the gravitational potential wells of the host galaxies. Both these effects would lower the fraction of radiative transfer modeling by GA17 have preferentially higher outflowing gas that escapes the galaxies. On the other hand, we also assumethat the outflowing gas is no longer being accelerated, which may not be the case if the winds are driven by the outward radiation pressure on dust grains, especially in the event of high far-IR optical depths and/or cosmic-ray

> Figure 15 shows the cumulative outflow mass for each object to the estimated escape velocity. We find typical galaxy escape fractions ~20% with large variation within the sample. The three objects with estimated escape fractions >25% are SPT2132-58 and SPT2311-54, which have the fastest outflows mass given its outflow velocity (or an atypically fasoutflow given its mass). Only □10% of the outflowing gas is traveling at 1.5 times the escape velocity or faster, and essentially none is traveling at twice the escape velocity.

Figure 15 also shows these escape fractions as a function of $L_{\rm IR}$, now including the local galaxy samples with stellar velocity dispersion measurement available to estimate the escape velocities. The uncertainties on the escape fractions sufficiently high velocity to escape the galaxy or even the dark include only those due to the uncertain escape velocities, but do not include the (unknown) contribution from any variations in the equivalentwidth to outflow mass proportionality (or the CO-H₂ conversion factor for the CO-based masses). We find a ≈0% up to 60%, reflective of the large range in outflow velocities and a rather limited dynamic range in galaxy mass. other observables,in agreementwith our conclusions in Section 4.1.

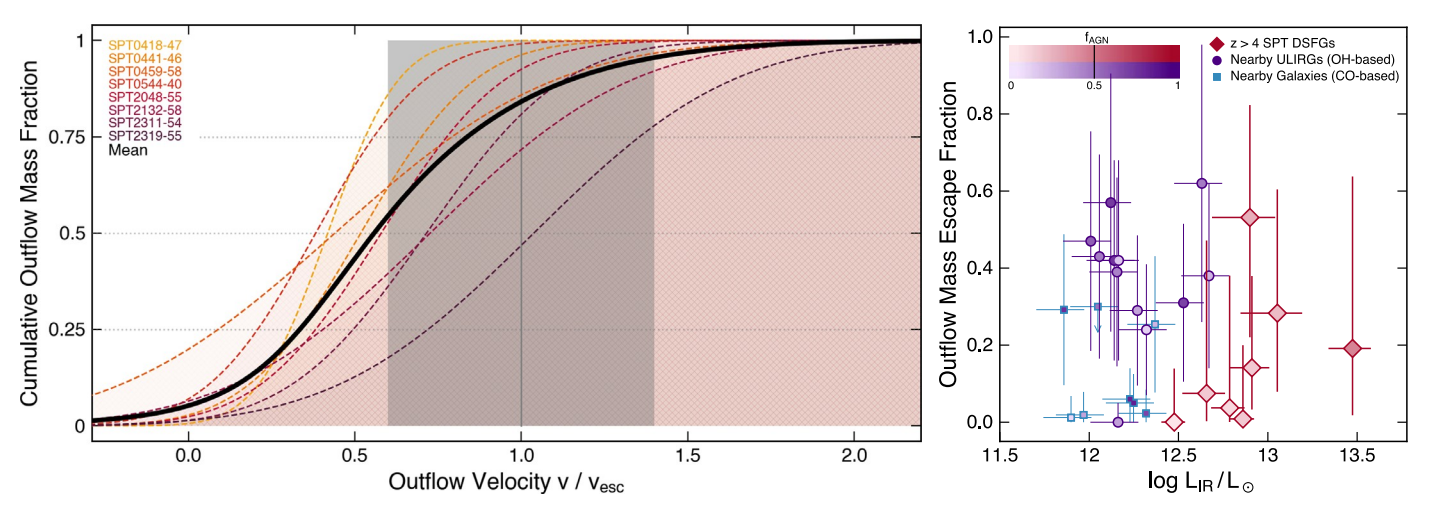


Figure 15. Left: cumulative molecular outflow masses as a function of the outflow velocity normalized to the galaxy escape velocity of each object; material moving V > V_{esc} will leave the galaxy and enter the CGM. The thick black line shows the mean of the individual sample objects, while the vertical shaded region shows the approximate uncertainty on the escape velocities. Right: fraction of the outflowing material that will escape into the CGM as a fundational solution and colorcoding as in Figure 7. On average only ≈20% of the molecular gas in the z□>□4 DSFG winds we have observed is traveling fast enough to leave the host galaxie there is wide dispersion in this fraction within the sample.

The galaxy outflow escape fractions in Figure 15 are substantially higher than those found by Fluetsch et al. (2019) even for the same objects. As discussed in Section 4.2, this is because those authors count the full broad CO component as belonging to the molecular outflows, thereby including a substantial amount of CO flux at systemic velocities that need not actually be outflowing. This additional flux (and therefore mass) artificially lowers the galaxy escape fractions well below the values we obtain following the more conservative definition of Lutz et al. (2020), who only considered the flux in the broad line wings in the outflow definition (excluding the core emission at systemic velocities). This more conservativedefinition results in total outflow masses a factorof ≈5 lower on average for the CO-based objects in Figure 15 and consequently higher escape fractions of the SPT DSFGs, we expect ~few ⁰ € of the outflowing compared to those found by Fluetsch et (2019).

While the uncertainties are large, the nearby ULIRGs in Figure 15 tend to show somewhat larger escape fractions than our own sample of high-redshift objects. These sources have $a_{unknown}$. Based on a sample of three $z\sim 2\,$ DSFGs with our own sample. As previously discussed his is most likely due to the fact that the sourceswith available OH-based fastest outflows (Figure 6). Given the lack of correlation between outflow velocity and stellar velocity dispersion or stellar mass over the limited dynamic range probed by these samples(e.g., Veilleux et al. 2013), this results in outflow escape fractions skewed toward larger values. As in Section 4.4, we expect that a more complete sample of local escape fractions werfd for the high-redshift DSFGs.

The bulk of the molecular gas in the outflows is destined to remain within the galaxies where it can become available for future star formation through a galactic fountain flow. At least in the cold molecular phase, most of the gas will not be permanently expelled and therefore these outflows cannot really be responsible for the very low gas fractions that are one²¹ of the hallmarks of quenched galaxies at lower redshifts (e.g., Young et al. 2011; Davis et al. 2016; Spilker et al. 2018a; Bezanson et al. 2019). Moreover, without continuous injection ease of observational comparison.

of thermal energy or turbulence over the long terthe CGM gas will develop a cooling flow resulting in significant gas accretion (e.g.Su et al. 2020).

4.6. Implications for CGM Enrichment

Finally, we consider the impact of the outflowing molecular gas that probably will escape in the context of the CGM surrounding these high-redshifDSFGs²⁰ The top panel of Figure 16 shows the mass of the molecular outflows traveling at speedsgreater than the galaxy escapevelocity in each source. We assumeall of this material enters the CGM, ignoring the loss of any materiathat escapes the larger dark matter halos (we expect this to be an exceedingly small fraction given the outflow velocity distributions in Figure 15). For most molecular gas to become incorporated into the CGM of the host halos.

The typical CGM properties of DSFGs are virtually mean and median escape fraction ≈40%, about double that forbackground quasar sightline absorption spectra, Fu et al. (2016) speculated that the CGM of DSFGs may be less massive and/ or that DSFGs inhabit somewhat less massive dark matter halos radiative transfer models are preferentially also those with the than co-eval quasars. However, given the much better statistics available for quasars at these redshifts Figure 16 shows the typical range of total cool (104 K) CGM gas mass within the virial radius of 2 < Z < 3 quasar hostpalaxies thoughto reside in $\log M_n M_{\odot} \sim 12$ –13 mass halos (Prochaska etal. 2014; Lau et al. 2016).²¹ Given the possible differences between the CGM of DSFGs and guasars and an expectation ULIRGs would show substantially more overlap with the lower that the CGM grows in mass from $z\Box^3$ 4 to z=2.5, we expect this range to be an approximate upper bound on the total cool CGM mass surrounding the higher-redshiftDSFGs in our sample.

²⁰ We consider the outflowing gas to be entering the CGM if its velocity is greater than the galaxy escape velocity, but less than the halo escape velocity. Warmer CGM phases are extremely difficult to observe in the distant universe Moreover, the thermalbalance of CGM phases is an active area of investigation and subject to numerical resolution effects in simulations (Hummels etal. 2019). We restrict our analysis to the coolCGM phase for

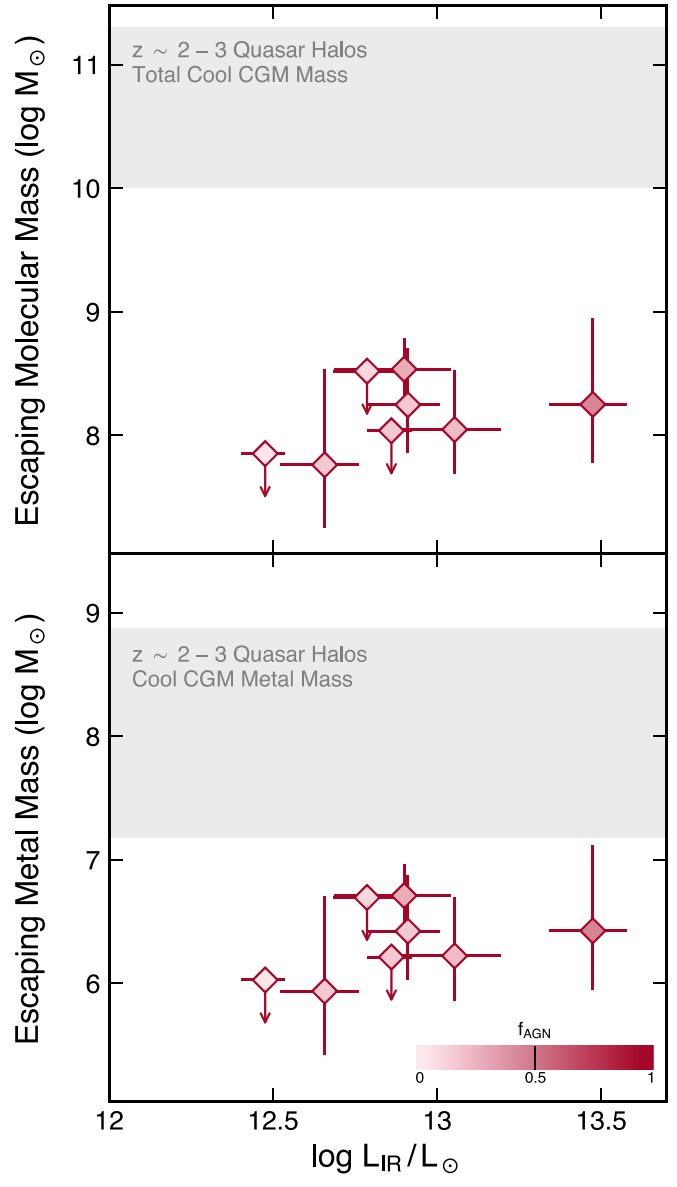


Figure 16. Estimates of the molecular gas mass (upper panel) and metal mass Hayward & Hopkins 2017; Pizzati et a2020). (lower panel) contained in the observed z□>□4 SPT DSFG outflowwithat escape the hostgalaxies and enter the surrounding CGM, assuming solar metallicity for the lower panel. For comparison, the gray shaded regions show the estimated total cool (10 104 K) CGM mass and metal mass surrounding quasarhost galaxies atslightly lower redshifts (Prochaska et al. 2014; Lau et al. 2016). The molecular phase of the outflow episodes we have observed conceivably contribute ~10% of the total metals contained in the CGM at later properties of the largestample of molecular outflows in the times but only a small fraction of the total cool gas.

The bottom panel of Figure 16 shows the total mass in metals being ejected into the CGM, under the simplifying assumption thatthe molecular outflows have approximately solar metallicity. If, as the outflow energetics suggest (Section 4.4), processes related to staformation are responsible for driving the molecular outflows, we may expect the outflowing gas to be enriched significantly beyond solar. moving the points upwards in the lower panel of Figure 16. In comparison the metallicity of the coolCGM gas surrounding 2 < Z < 3 quasars is subsolar, $Z \square \sim \square 0.1_{\overline{e}}$ 0.18k@ly because it is a mixture of metal-enriched outflow gasless metal-rich poor material accreting from the cosmic web (e.g. Muratov

et al. 2017; Hafen et al. 2019). The range of total CGM metal mass for the same $z\Box \sim \Box 2-3$ guasar samples is also shown in Figure 16.

Taken together, the two panels of Figure 16 give an intriguing (if admittedly speculative) picture of the relationship between molecular outflows and the CGM surrounding these galaxies.If the DSFGs in our sample will evolve to become like the quasars observed at slightly lower redshift, the current molecular outflow episodes will contribute only a small fraction \(\square\$ 1%-10% of the total cool CGM mass. Evidently the total CGM mass mustbe assembled from some combination of outflowing gas in warmer phasesthan we have observed,many repeated outflow events through the lifetime of the galaxies and accretion of additionatas into the CGM from the cosmic web or infalling satellites. While observations of the multiphase components of outflows are rare even in the nearby universe, it appears that in general the molecular phase contains a significant if not dominant portion of the total outflow mass (Fluetsch et al. 2019), so additional mechanisms beyond accounting for the unobserved warmer phases are likely required.On the other handthe currentoutflow episodes can contribute some substantial fraction ~10% or more of the total metals presentin the CGM at lower redshift. This fraction would rise further if the outflowing molecular gas is enriched beyond solar metallicity. X-ray observations of the hot plasma in nearby winds typically find α/Fe elemental abundance patterns (i.e., including oxygen, of relevance to our OH observations) enhanced to sevetimes the solar value (e.g., Nardini et al. 2013; Veilleux et al. 2014; Liu et al. 2019), though the composition of the molecular gas in outflows is unknown, even at low redshift.

The outflow metallicities of these highly obscured galaxies are conceivably observable with future observations of far-IR fine structure lines (e.g.Nagao et al. 2011; Pereira-Santaella et al. 2017). Indeed, the [CII] 158 mm line has recently been detected on 10-30 kpc spatial scales surrounding co-eval lower mass galaxies through stacking and, in a few cases, direct individual detections (Fujimoto et al. 2019, 2020; Ginolfi et al. 2020). These studies conclude that metal-enriched outflows are the most likely source of the extended [CII] emission, as generally expected from simulations (e.g., Muratov et al. 2015;

5. Conclusions

This work has focused primarily on deriving the physical early universe to date. These outflows, detected with ALMA as blueshifted absorption line wings in the ground-stateOH 119mm doublet, appear ubiquitous among massive, IRluminous DSFGs atz□>□We rely heavily on observations of outflows in low-redshift galaxies with much richer OH spectroscopic data available hich we use as a "training set" of objects to derive outflow rates for our high-redshift sample with only the ground-state OH lines observed. Comparing four methods for estimating outflow rates, we find agreement at the factor of 2 level. Future improvements in the outflow rate estimates will require either observations of shorter-wavelength OH lines (e.g., the 79nm doublet) and/or the much less abundant 80H isotopologue, both of which have far lower line opacities than the 119m doublet currently available. Though material stripped or ejected from infalling satellites, and metal- the uncertainties on the outflow rates (and therefore the other outflow properties derived from the outflow rates) are large, we

draw a number of conclusions from this first high-redshift outflow sample:

- 1. We find tentative evidence that the outflow velocity correlates with $_{IR}$ within the z \square > \square 4 sample (Figure 6 and Section 4.1). The same is not true for the combined lowredshift galaxies with OH dataA larger sample athigh legitimate difference between outflows in low- and highredshift objects.
- 2. We find high molecular outflow rate arranging from ~150–800 M_{\odot} yr⁻¹. This was not unexpected given the high IR luminosities of our sample. The wind mass loading factors are nevertheless slightly less than unity. other quantity including SFR of SFR. Gas consumption by star formation is more important than gas removal by outflows in regulating the molecular gas reservoirsof these objects (Figures 7 and 1Sections 4.2 and 4.3).
- 3. The cold molecular mass of the outflows is also high, $\log M_{\rm out}/M_{\odot}$ » 8.5-9. This still only represents 1%–10% galaxies (Figure 10 and Section 4.3).
- 4. We find only very modest momentum boostsin the outflows compared to the radiative momentum, $P_{\text{out}}/(L/C)$ < 3. These boosts are fully achievable by winds driven either by supernovae or radiation pressure on dust grains. The outflow kinetic energy fluxes, similarly, are always less than the expected maximum values for outflows driven by star formation. There is no System. need for partially or fully energy-conserving wind phases (Figures 13 and 14Section 4.4).
- 5. Following the previous conclusion, the outflows we have (Spilker et al. 2016), ripples (Hezaveh observed do not require an additional injection of momentum or energy from AGN in these While we currently have no evidence for AGN activity in our sample objects with limits from rest-frame mid-IR photometry, we cannot rule out that deeply buried AGN are present. The outflow energetics, however, do not require an AGN as the primary driving source.
- 6. We estimate that ≈20% of the gas in the molecular outflows is traveling fastenough to escape the galaxies and enter the CGM, on average, though with large uncertaintiesand a range from 0%-50% within the sample. While an admittedly more speculative conclusion, we find that the molecular material moving fast enough to escape the galaxies represents only a small fraction of the total cool CGM mass but perhaps 10% of Christopher CHayward https://orcid.org/0000-0003the metal mass observed in the CGM of massive halos at 4073-3236 slightly lower redshifts (Figures 15 and 1 Sections 4.5 and 4.6).

While we have presented the largest currently available sample of molecular outflows at $z\square>\square i4$, is by no means a cleanly selected or complete sample; our primary selection criterion was merely thathe redshift of each targetplace the OH 119 nm lines in an atmospheric window for ALMA observations. Given the high success rate in detecting outflows Xxel Weiß https://orcid.org/0000-0003-4678-3939 in these galaxieswe hope to have motivated future observations of samples that span a wider range in galaxy properties in order to build a more comprehensive view of the statistical properties of molecular outflows in the early universe. The physical properties derived forthe outflows assembled from

our present sample and future samples will provide invaluable constraints for simulations of galaxy evolution, tracking the prevalence and consequences of olecular outflows through

We thank the referee for a thorough and constructive report that improved the quality of this paped.S.S.is supported by redshift will be necessary to determine whether there is a NASA Hubble Fellowship grant #HF2-51446 awarded by the Space Telescope Science Institute hich is operated by the Association of Universities for Research in Astronomylnc., for NASA, under contract NAS5-26555. K.C.L., D.P.M., K.P., and J.D.V. acknowledge supportfrom the US NSF under grants AST-1715213 and AST-1716127. This work was performed in partat the Aspen Centerfor Physics, which is The mass loading factors do not clearly correlate with any supported by National Science Foundation grant PHY-1607611.

This paper makes use of the following ALMA data: ADS/ JAO.ALMA#2015.1.00942.S, ADS/JAO. ALMA#2016.1.00089.S, ADS/JAO.ALMA#2018.1.00191. S, and ADS/JAO.ALMA#2019.1.00253.S. ALMA is partnership of ESO (representing its member states), NSF of the total molecular gas mass of these gas-rich massive(USA) and NINS (Japan), together with NRC (Canada), MOST and ASIAA (Taiwan), and KASI (Republic of Korea), in cooperation with the Republic of Chile. The Joint ALMA Observatory is operated by ESO, AUI/NRAO and NAOJ. The National Radio Astronomy Observatory is a facility of the National Science Foundation operated under cooperative agreement by Associated Universitiesc.

This research has made use of NASA's Astrophysics Data

Facility: ALMA.

Software: CASA (McMullin et al. 2007), visilens et al. 2016), astropy (Astropy Collaboration et al. 2018), matplotlib (Hunter 2007).

ORCID iDs

Justin S.Spilker https://orcid.org/0000-0003-3256-5615 Manuel Aravena https://orcid.org/0000-0002-6290-3198 Kedar A. Phadken https://orcid.org/0000-0001-7946-557X Matthieu Béthermin https://orcid.org/0000-0002-3915-2015

Chenxing Dong

(董辰兴) https://orcid.org/0000-0002-5823-0349 Anthony H. Gonzalez https://orcid.org/0000-0002-0933-8601

Yashar D.Hezaveh https://orcid.org/0000-0002-8669-5733 Katrina C. Litke https://orcid.org/0000-0002-4208-3532 Matthew A. Malkan https://orcid.org/0000-0001-6919-1237

Daniel P. Marrone https://orcid.org/0000-0002-2367-1080 Desika Narayanan https://orcid.org/0000-0002-7064-4309 Cassie Reuter https://orcid.org/0000-0001-7477-1586 Joaquin D.Vieira https://orcid.org/0000-0001-7192-3871

References

Agertz, O., & Kravtsov, A. V. 2016, ApJ, 824, 79 Aravena, M., Spilker, J. S., Bethermin, M., et al. 2016, MNRAS, 457, 4406

```
Arribas, S., Colina, L., Bellocchi, E., Maiolino, R., & Villar-Martín, M. 2014,
   A&A, 568, A14
Astropy Collaboration Price-Whelan A. M., Sipőcz, B. M., et al. 2018, AJ,
Barro, G., Kriek, M., Pérez-González, G., et al. 2016, ApJL, 827, L32
Bezanson,R., Spilker, J., Williams, C. C., et al. 2019, ApJL, 873, L19
Bolatto, A. D., Wolfire, M., & Leroy, A. K. 2013, ARA&A, 51, 207
Brennan, R., Choi, E., Somerville, R. S., et al. 2018, ApJ, 860, 14
Calderón, D., Bauer, F. E., Veilleux, S., et al. 2016, MNRAS, 460, 3052
Chevalier, R. A., & Clegg, A. W. 1985, Natur, 317, 44
Chisholm, J., Tremonti, C. A., Leitherer, C., et al. 2015, ApJ, 811, 149
Cicone, C., Maiolino, R., Sturm, E., et al. 2014, A&A, 562, A21
Costa, T., Sijacki, D., & Haehnelt, M. G. 2014, MNRAS, 444, 2355
Davé, R., Anglés-Alcázar, D., Narayanan, D., et al. 2019, MNRAS, 486, 2827 Pickett, H. M., Poynter, R. L., Cohen, E. A., et al. 1998, JQSRT, 60, 883
Davis, T. A., Greene, J., Ma, C.-P., et al. 2016, MNRAS, 455, 214
Fabian, A. C. 1999, MNRAS, 308, L39
Faucher-GiguèreC.-A., & Quataert, E. 2012, MNRAS, 425, 605
Fischer, J., Sturm, E., González-Alfonso E., et al. 2010, A&A, 518, L41
Fluetsch, A., Maiolino, R., Carniani, S., et al. 2019, MNRAS, 483, 4586
Fu, H., Hennawi, J. F., Prochaska J. X., et al. 2016, ApJ, 832, 52
Fujimoto, S., Ouchi, M., Ferrara, A., et al. 2019, ApJ, 887, 107
Fujimoto, S., Silverman, J. D., Bethermin, M., et al. 2020, ApJ, 900, 1
Gebhardt,K., Bender,R., Bower, G., et al. 2000, ApJL, 539, L13
Ginolfi, M., Jones, G. C., Béthermin, M., et al. 2020, A&A, 633, A90
Goicoechea J. R., & Cernicharo, J. 2002, ApJL, 576, L77
González-Alfonso, E., Fischer, J., Spoon, H. W. W., et al. 2017, 11
Hafen, Z., Faucher-Giguère. - A., Anglés-Alcázar D., et al. 2019, MNRAS,
   488, 1248
Harrison, C. M., Alexander, D. M., Mullaney, J. R., & Swinbank, A. M. 2014,
   MNRAS, 441, 3306
Hayward, C. C., & Hopkins, P. F. 2017, MNRAS, 465, 1682
Hayward, C. C., Sparre, M., Chapman, S. C., et al. 2020, arXiv:2007.01885
Heckman, T. M., Alexandroff, R. M., Borthakur, S., Overzier, R., &
   Leitherer, C. 2015, ApJ, 809, 147
Heckman, T. M., & Borthakur, S. 2016, ApJ, 822, 9
Herrera-CamusR., Sturm, E., Graciá-CarpioJ., et al. 2020, A&A, 633, L4
Hezaveh,Y. D., Dalal, N., Marrone,D. P., et al. 2016, ApJ, 823, 37
Hummels, C. B., Smith, B. D., Hopkins, P. F., et al. 2019, ApJ, 882, 156
Hunter, J. D. 2007, CSE, 9, 90
King, A., & Pounds, K. 2015, ARA&A, 53, 115
Lau, M. W., ProchaskaJ. X., & Hennawi, J. F. 2016, ApJS, 226, 25
Leroy, A. K., Walter, F., Martini, P., et al. 2015, ApJ, 814, 83
Liu, W., Veilleux, S., Iwasawa, K., et al. 2019, ApJ, 872, 39
Long, A. S., Cooray, A., Ma, J., et al. 2020, ApJ, 898, 133
Lutz, D., Berta, S., Contursi, A., et al. 2016, A&A, 591, A136
Lutz, D., Shimizu, T., Davies, R. I., et al. 2018, A&A, 609, A9
Lutz, D., Sturm, E., Janssen A., et al. 2020, A&A, 633, A134
Ma, J., Gonzalez A. H., Vieira, J. D., et al. 2016, ApJ, 832, 114
Mangum, J. G., & Shirley, Y. L. 2015, PASP, 127, 266
Marrone, D. P., Spilker, J. S., Hayward, C. C., et al. 2018, Natur, 553, 51 McMullin, J. P., Waters, B., Schiebel, D., Young, W., & Golap, K. 2007, in
   ASP Conf. Ser. 376, Astronomical Data Analysis Software and Systems
   XVI, ed. R. A. Shaw, F. Hill, & D. J. Bell (San Francisco, CA: ASP), 127
Miller, T. B., Chapman S. C., Aravena, M., et al. 2018, Natur, 556, 469
Müller, H. S. P., Schlöder, F., Stutzki, J., & Winnewisser, G. 2005, JMoSt,
   742, 215
```

```
Müller, H. S. P., Thorwirth, S., Roth, D. A., Winnewisser, G. 2001, A&A,
  370, L49
Muratov, A. L., Kereš, D., Faucher-Giguère C.-A., et al. 2015, MNRAS,
  454, 2691
Muratov, A. L., Kereš, D., Faucher-Giguère C.-A., et al. 2017, MNRAS,
   468,4170
Murphy, E. J., Condon, J. J., Schinnerer E., et al. 2011, ApJ, 737, 67
Murray, N., Ménard, B., & Thompson, T. A. 2011, ApJ, 735, 66
Murray, N., Quataert E., & Thompson, T. A. 2005, ApJ, 618, 569
Nagao, T., Maiolino, R., Marconi, A., & Matsuhara, H. 2011, A&A, 526, A149
Nardini, E., Wang, J., Fabbiano, G., et al. 2013, ApJ, 765, 141
Pereira-SantaellaM., Rigopoulou, D., Farrah, D., Lebouteiller, V., & Li, J.
   2017, MNRAS, 470, 1218
Pizzati, E., Ferrara A., Pallottini, A., et al. 2020, MNRAS, 495, 160
Planck Collaboration, Ade, P. A. R., Aghanim, N., et al. 2016, A&A, 594, A13
ProchaskaJ. X., Lau, M. W., & Hennawi, J. F. 2014, ApJ, 796, 140
Reuter, C., Vieira, J. D., Spilker, J. S., et al. 2020, ApJ, 902, 78
Richings, A. J., & Faucher-Giguère C.-A. 2018, MNRAS, 474, 3673
Roberts-Borsani, G. W., & Saintonge, A. 2019, MNRAS, 482, 4111
Rubin, K. H. R., ProchaskaJ. X., Koo, D. C., et al. 2014, ApJ, 794, 156
Rupke, D. S., Veilleux, S., & Sanders, D. B. 2005, ApJS, 160, 115
Scannapieco 2013, ApJL, 763, L31
Schneider E. E., & Robertson, B. E. 2017, ApJ, 834, 144
Silk, J., & Rees, M. J. 1998, A&A, 331, L1
Somerville, R. S., & Davé, R. 2015, ARA&A, 53, 51
Spilker, J., Bezanson R., Barišić, I., et al. 2018a, ApJ, 860, 103
Spilker, J. S., Aravena, M., Béthermin, M., et al. 2018b, Sci, 361, 1016
Spilker, J. S., Aravena, M., Marrone, D. P., et al. 2015, ApJ, 811, 124
Spilker, J. S., Bezanson, R., Weiner, B. J., Whitaker, K. E., & Williams, C. C.
  2019, ApJ, 883, 81
Spilker, J. S., Marrone, D. P., Aravena, M., et al. 2016, ApJ, 826, 112
Spilker, J. S., Phadke, K. A., Aravena, M., et al. 2020, ApJ, 905, 85
Spoon, H. W. W., Farrah, D., Lebouteiller, V., et al. 2013, ApJ, 775, 127
Stone, M., Veilleux, S., Meléndez, M., et al. 2016, ApJ, 826, 111
StraatmanC. M. S., Labbé, I., Spitler, L. R., et al. 2014, ApJL, 783, L14
Su, K.-Y., Hopkins, P. F., Hayward, C. C., et al. 2020, MNRAS, 491, 1190
Tacchella, S., Carollo, C. M., Renzini, A., et al. 2015, Sci, 348, 314
Thompson, T. A., Fabian, A. C., Quataert, E., & Murray, N. 2015, MNRAS,
  449, 147
Thompson, T. A., Quataert, E., & Murray, N. 2005, ApJ, 630, 167
Thompson, T. A., Quataert, E., Zhang, D., & Weinberg, D. H. 2016, MNRAS,
  455, 1830
Toft, S., Smolčić, V., Magnelli, B., et al. 2014, ApJ, 782, 68
Tombesi, F., Meléndez, M., Veilleux, S., et al. 2015, Natur, 519, 436
Tumlinson, J., Peeples, M. S., & Werk, J. K. 2017, ARA&A, 55, 389
Veilleux, S., Bolatto, A., Tombesi, F., et al. 2017, ApJ, 843, 18
Veilleux, S., Cecil, G., & Bland-Hawthorn, J. 2005, ARA&A, 43, 769
Veilleux, S., Maiolino, R., Bolatto, A. D., & Aalto, S. 2020, A&ARv, 28, 2
Veilleux, S., Meléndez, M., Sturm, E., et al. 2013, ApJ, 776, 27
Veilleux, S., Teng, S. H., Rupke, D. S. N., Maiolino, R., & Sturm, E. 2014,
   ApJ, 790, 116
Weiner, B. J., Coil, A. L., Prochaska J. X., et al. 2009, ApJ, 692, 187
Wold, H. 1966, in Multivariate Analysis, ed. P. R. Krishnajah (New York:
   Academic Press), 391
```

Young, L. M., Bureau, M., Davis, T. A., et al. 2011, MNRAS, 414, 940

Zubovas, K., & King, A. 2012, ApJL, 745, L34